THE ASTROPHYSICAL JOURNAL, 423:94–115, 1994 March 1

CLUMPED X-RAY EMISSION AROUND RADIO GALAXIES IN ABELL CLUSTERS

JACK O. BURNS AND GEORGE RHEE[1]
Department of Astronomy, New Mexico State University, Las Cruces, NM 88003; e-mail: jburns@nmsu.edu
FRAZER N. OWEN
National Radio Astronomy Observatory,[2] P.O. Box 0, Socorro, NM 87801; e-mail: fowen@pilabo.aoc.nrao.edu
AND
JASON PINKNEY
Department of Astronomy, New Mexico State University, Las Cruces, NM 88003; e-mail: jpinkney@nmsu.edu
Received 1993 May 19; accepted 1993 September 13

ABSTRACT

We have made a comparison of the X-ray and radio morphologies for a sample of 41 rich cluster fields using *Einstein Observatory* IPC and VLA 20 cm images. Surprisingly, we find that 75% of the radio galaxies have a statistically significant X-ray peak or subclump within 5′ of the radio galaxy position. The X-ray luminosity and the generally extended nature of the X-ray subclumps suggest that these subclumps are overdense regions emitting free-free radiation, although there is also evidence for AGN X-ray emission coming from some of the more compact, high surface brightness X-ray peaks. Some interesting correlations with radio morphology were also discovered. For clusters which contain wide-angle–tailed radio sources associated with centrally dominant galaxies, there are significant elongations or clumps in the central X-ray emission which are unusual for this type of cluster. We suggest that cluster radio galaxies are pointers to particular clusters or regions within clusters that have recently undergone mergers between cluster subsystems.

Subject headings: galaxies: clustering — galaxies: interactions — radio continuum: galaxies — X-rays: galaxies

1. INTRODUCTION

During the last decade, extensive radio-frequency surveys of clusters of galaxies have been made using the VLA and Westerbork radio telescopes at 20 cm. Hundreds of radio sources identified with galaxies in rich (e.g., Zhao, Burns, & Owen 1989; Owen, White, & Burns 1992; Owen, White, & Ge 1993; Fanti et al. 1983a, b) and poor (e.g., Burns et al. 1987) clusters have been imaged. From investigations of the statistics of cluster radio galaxy emission, several interesting questions and surprising results have emerged concerning the nature of the radio sources and their environs. These questions include the following:

1. Why is the shape of the radio luminosity function (Fanti 1984) virtually identical for radio galaxies inside and outside of rich clusters? One might naively expect, for example, that the higher confining thermal gas pressure within the intracluster medium (ICM) would produce larger magnetic field energy densities and higher radio luminosities for cluster sources. This is not observed.

2. Why does the probability of radio emission from a galaxy not depend upon global cluster galaxy density (e.g., Zhao et al. 1989)? One might have anticipated more galaxy interactions and thus more radio-loud galaxies as cluster richness increased. Again, this is not observed. Furthermore, radio sources are *not* primarily identified with the brightest cluster member but are associated with a range of galaxy optical luminosities.

3. Why is the distribution of projected distances of radio galaxies from the cluster centers very peaked on Abell's positions for the clusters? Cluster radio galaxies are more centrally concentrated than either the optical or X-ray emission (see § 3.2).

4. Why are tailed radio sources found in both rich and poor clusters? The U-shaped jets in rich cluster head-tail radio sources (e.g., O'Dea & Owen 1985) are believed to be bent by dynamic pressure ($\rho_{\rm ICM} v_g^2$) resulting from transonic motion of the radio galaxy through the ICM (e.g., Jones & Owen 1979; O'Dea 1985). This dynamic pressure is reduced by factors of 10–100 in poor clusters because of the smaller gas densities (Burns, Gregory, & Holman 1981) and lower velocity dispersions in poor clusters; it is insufficient to bend the radio jets/tails to the observed curvature (Eilek et al. 1984; Stocke & Burns 1987). Yet spectacular versions of head-tail sources are found in poor clusters.

The answers to the above questions must hinge in large part on the gaseous environments near radio galaxies in clusters. The surrounding hot gas both confines (via either thermal or dynamic pressure) and shapes the extended radio plasma. X-ray images are the best probes of the hot gas around radio galaxies, enabling us to study in detail the range of environmental conditions surrounding radio sources in rich clusters. So the key to answering these questions may lie in the comparison of X-ray and radio emission in and around radio galaxies in clusters.

We have begun by correlating our extensive VLA radio survey of Abell clusters with the *Einstein* X-ray database for clusters with larger than 2′ diameter radio sources. We report on the results of this correlative study in this paper. In future papers we will consider other clusters with smaller radio sources, and we will explore correlations between our sta-

[1] Postal address: Department of Physics, University of Nevada, Las Vegas, NV 89154.

[2] The National Radio Astronomy Observatory is operated by Associated Universities, Inc., under cooperative agreement with the National Science Foundation.

tistically complete VLA database and the *ROSAT* all-sky survey.

This paper is organized as follows. In § 2 the *Einstein*/VLA image comparisons are discussed. We define the sample and present X-ray/radio overlays for each cluster. In § 3 we describe the results qualitatively and quantitatively. We also discuss the possible origins of the X-ray clumped emission. We present our conclusions in § 4. Comments on the X-ray, radio, and optical properties of individual clusters are given in the Appendix. We assume $H_0 = 75$ km s^{-1} Mpc^{-1} and $q_0 = 0.1$ throughout this paper.

2. *Einstein*/VLA IMAGE COMPARISONS

In this section we describe the sample, discuss the method of data analysis, and present the X-ray/radio overlays.

2.1. *Sample and Data Analysis*

Our sample is drawn from the northern Abell cluster catalog (Abell 1958). We are in the process of completing a 20 cm VLA survey of radio galaxies within one-half of a corrected Abell radius (Owen et al. 1982) of the cluster center. We have defined two samples from the radio survey (Owen et al. 1992): (1) radio galaxies with $S_{20} > 10$ mJy and $z < 0.09$, and (2) radio galaxies with $S_{20} > 200$ mJy which lie in any northern Abell (1958) cluster (generally with $z < 0.2$). All these radio galaxies have measured redshifts and/or optical magnitudes that are consistent with cluster membership. In Paper I (Zhao et al. 1989), the properties of the nearby radio sources in clusters with Abell distance class ≤ 3 were described. In Paper II (Owen et al. 1992) and III (Owen et al. 1993), images and optical identifications for the generally more distant radio sources in the above two samples were presented.

For the purposes of comparing the radio and X-ray properties in Abell clusters, we have selected a subsample from the VLA survey which contains radio sources having angular sizes greater than 2′. Since the *Einstein* Imaging Proportional Counter (IPC) resolution is $\approx 1.'7$ (FWHM) and we are interested in comparing the radio and X-ray morphologies, only clusters with significantly extended radio sources were selected. We have cross-correlated the *Einstein* database with the positions of the extended radio galaxies; we then selected X-ray fields which have radio galaxies inside the ribs of the IPC ($\approx 30'$ from the field center). Although most IPC fields were targeted on the Abell cluster, some clusters were observed serendipitously as part of other programs.

Our sample consists of 49 radio sources in 41 Abell clusters for which *Einstein* IPC maps are available. We note that although our VLA survey is statistically complete, the *Einstein* database on Abell clusters is not. However, we believe that this sample of 41 clusters is generally representative of the variety of X-ray and radio morphologies found in rich clusters.

We used the *Einstein* IPC images provided by CfA on CD ROM (Harris et al. 1990); they have a field of view of $60' \times 60'$ with an angular resolution of $\approx 1.'7$ FWHM (after smoothing with a two-dimensional Gaussian) (see, e.g., Mauche & Gorenstein 1986). With these detector characteristics, the corresponding linear scales at $z = 0.05$ are $60' \approx 3.5$ Mpc and $1.'7 \approx 100$ kpc. The pixel size of these images is 24″. The data for these images were summed over a bandwidth 0.3–4.5 keV. The data were background-subtracted and corrected for vignetting using standard software at CfA.

The typical field of view of the VLA images is $40' \times 40'$, and the FWHM resolution of the synthesized beam at 20 cm is $\approx 15''$. The corresponding pixel size of the VLA maps is 5″. For more details of the VLA imaging see Papers I–III. For the larger sources, some source flux density is missing, owing to incomplete sampling of the (u, v)-plane at small baselines (see, e.g., Zhao et al. 1989).

In Table 1 we present the sample and its properties. Column (1) lists the Abell number. Column (2) lists the cluster redshift from the compilations of Struble & Rood (1991), Owen, White, & Thronson (1988), and Owen, Ledlow, & Keel (1994b). Columns (3) and (4) list the radio source right ascension and declination (epoch 1950). The radio source position is taken to be the optical position of the galaxy identified with the radio source. Column (5) lists the total radio power in W Hz^{-1} at 20 cm. Column (6) lists the radio source morphology (NAT = narrow-angle–tailed radio galaxy; WAT = wide-angle–tailed radio galaxy; TJ = twin jet radio galaxy; CPX = complex; BTJ = bent twin jet; D = double-lobed; Diff = diffuse). Columns (7) and (8) list the X-ray right ascension and declination (epoch 1950); the X-ray position is taken to be the closest significant peak of X-ray emission to the radio galaxy position (see below). Column (9) lists the cluster X-ray luminosity (0.3–4.5 keV) in ergs s^{-1} calculated as discussed below. Column (10) lists the position angle of the cluster X-ray emission as fitted by a two-dimensional ellipse. Column (11) lists the position angle of the radio source. Column (12) lists the separation (in Mpc) between the closest, significant peak of X-ray emission and the optical position of the galaxy associated with the radio emission. Column (13) gives the radius of the X-ray clump (in arcseconds) closest to the radio galaxy and column (14) its X-ray luminosity. Column (15) lists the signal-to-noise ratio determined by comparing the X-ray counts within the X-ray clump with those in an annulus surrounding the clump. Finally, column (16) is an estimate of the clump density (in cm^{-3}) assuming the X-ray emission is free-free emission as discussed in § 3.3.

The cluster X-ray luminosities (col. [9]) were calculated from the *Einstein* IPC frames as follows. First, the X-ray surface brightness (counts s^{-1} arcmin^{-2}) was derived by dividing each image by the live time. The live time is the total number of seconds during which the detectors were able to collect data. For *Einstein* X-ray images, corrections in the live time have been made for intervals lost because of Earth occultation, passage through the South Atlantic Anomaly, and detector dead time. Second, we chose to calculate cosmologically corrected isophotal luminosities to facilitate comparisons between clusters. Using trial and error, we settled on a minimum isophotal level of 3×10^{-3} counts s^{-1} arcmin^{-2}. However, we were unable to use this criterion on all clusters. For several nearby clusters (e.g., Coma), the X-ray emission fills the IPC field of view, and this minimum brightness level was not seen on the IPC image. For a few other clusters, the X-ray surface brightness was too low to meet this criterion anywhere. The NRAO AIPS task TVSTAT was used to measure the total X-ray count rate within the often irregular minimum isophotal contour after converting between counts s^{-1} arcmin^{-2} and counts s^{-1} pixel^{-1}. Third, the conversion between count rate and energy flux (ergs s^{-1} cm^{-2}) for the *Einstein* IPC weakly depends on the intrinsic source spectrum. The flux was calculated over the energy band 0.3–4.5 keV using an assumed Raymond & Smith (1977) spectral distribution with a temperature of 3 keV for all clusters (over this energy band, such an assumption introduces relatively small errors in F_X). This flux was further corrected for Galactic photoelectric absorp-

TABLE 1

THE SAMPLE

Abell	z	radio α (1950.0)	radio δ	P_{20}	radio morph	X-ray α (1950.0)	X-ray δ	L_X	θ_X	θ_R	δr	Rx_{clump} "	Lx_{clump}	σ_{clump}	n_{clump}
(1)	(2)	(3)	(4)	(5)	(6)	(7)	(8)	(9)	(10)	(11)	(12)	(13)	(14)	(15)	(16)
74	0.0654	00 36 39.0	-22 36 30.2	1.10×10^{24}	NAT?	00 36 37.2	-22 37 02	1.07×10^{43}	140	0	0.05	99	7.30×10^{42}	cc	0.0021
75	0.0622	00 37 04.4	20 57 39.2	1.10×10^{24}	D	00 37 07.5	20 55 59	4.48×10^{42}	88	34	0.29	71	1.89×10^{42}	4.3	0.0018
98	0.1054	00 43 50.8	20 11 41.6	1.28×10^{25}	WAT	00 43 48.3	20 11 48	1.29×10^{43}	135	174	0.07	78	4.64×10^{42}	4.9	0.0012
114	0.0587	00 50 58.0	-22 00 30.2	6.65×10^{24}	TJ	00 50 59.8	-22 00 58	1.11×10^{42}	20	52		52	1.90×10^{41}	2.0	0.0010
133	0.0566	01 00 15.3	-22 09 03.6	1.02×10^{24}	CPX	01 00 15.2	-22 08 48	4.19×10^{43}		65	0.02	151	6.92×10^{42}	cc	0.0152
160	0.0444	01 10 20.5	15 13 35.0	2.79×10^{24}	WAT	01 10 25.2	15 13 48	3.36×10^{42}		65	0.06	74	3.97×10^{41}	2.3	0.0043
194	0.0180	01 23 11.5	-01 38 24.5	5.70×10^{23}	NAT	01 23 13.6	-01 38 37	1.14×10^{43}	140	20	0.01	93	6.35×10^{40}	4.8	0.0013
		01 23 27.6	-01 36 18.9	2.05×10^{24}	TJ	01 23 26.4	-01 36 13	1.14×10^{43}		10	0.01	90	1.48×10^{41}	8.1	0.0021
400	0.0238	02 55 03.1	05 49 20.9	3.07×10^{24}	TJ	02 54 59.0	05 48 59	4.60×10^{42}	60	40	0.03	167	2.24×10^{42}	cc	0.0022
		02 55 03.0	05 49 37.0	3.07×10^{24}	TJ	02 54 59.0	05 48 59	4.60×10^{42}	60	40	0.03	167	2.24×10^{42}	cc	0.0022
401	0.0748	02 55 47.1	13 22 22.8	4.72×10^{24}	NAT	02 56 15.2	13 23 32	1.57×10^{44}	10	0	0.56	138	4.28×10^{43}	cc	0.0025
407	0.0463	02 58 44.0	35 38 35.2	3.28×10^{24}	CPX	02 58 46.8	35 38 48	2.57×10^{43}	25	40	0.04	80	3.12×10^{41}	cc	0.0009
415	0.0788	03 04 29.4	-12 17 55.0	6.12×10^{24}	NAT?	03 04 26.4	-12 18 00	3.24×10^{43}	120	105	0.06	80	1.13×10^{43}	cc	0.0027
514	0.0734	04 45 53.0	-20 31 52.3	1.03×10^{24}	NAT	04 45 49.6	-20 31 23	2.03×10^{43}	115	30	0.10	61	1.17×10^{42}	6.1	0.0014
		04 46 00.4	-20 30 10.8	1.29×10^{24}	NAT	04 45 58.1	-20 31 46	2.03×10^{43}	120	80	0.23	75	1.22×10^{42}	5.2	0.0010
		04 46 20.7	-20 37 26.0	5.44×10^{24}	NAT?	04 46 20.4	-20 38 34	2.03×10^{43}	170	35	0.09	62	5.73×10^{41}	4.1	0.0001
568	0.0751	07 04 22.7	35 08 13.9	3.18×10^{24}	NAT		no detection	$< 2.34 \times 10^{42}$					$< 1.05 \times 10^{42}$		
		07 04 24.3	35 08 22.9	2.90×10^{24}	TJ		no detection	$< 2.34 \times 10^{42}$					$< 1.05 \times 10^{42}$		
		07 04 18.2	35 09 49.0	7.38×10^{23}	NAT		no detection	$< 2.34 \times 10^{42}$					$< 1.05 \times 10^{42}$		
569	0.0196	07 05 21.4	48 41 47.0	6.99×10^{23}	BTJ	07 05 22.8	48 41 37	1.22×10^{43}	55	75	0.01	81	8.57×10^{41}	cc	0.0052
629	0.1459	08 10 10.1	66 35 58.2	1.20×10^{25}	NAT	08 10 15.9	66 35 48	1.58×10^{43}	105	110	0.19	99	1.58×10^{42}	cc	0.0003
		08 10 25.3	66 34 28.8	5.10×10^{23}	NAT	08 10 15.9	66 35 48	1.58×10^{43}	105	140	0.19	99	1.58×10^{42}	cc	0.0003
690	0.0788	08 36 13.5	29 01 13.1	1.28×10^{25}	WAT	08 36 11.1	29 01 47	9.00×10^{41}	125	140	0.07	90	9.00×10^{41}	cc	0.0006
780	0.0540	09 15 41.4	-11 53 08.2	2.64×10^{26}	WAT	09 15 40.0	-11 52 47	2.08×10^{44}	60	40	0.03	155	2.08×10^{43}	cc	0.0073
1234	0.1663	11 19 51.6	21 40 49.1	3.20×10^{25}	CPX	11 19 50.4	21 39 58	7.94×10^{43}	145	100	1.14	73	3.61×10^{43}	3.1	0.0032
1308	0.0484	11 30 31.7	-03 44 12.5	3.66×10^{24}	TJ		no detection	$< 4.06 \times 10^{41}$					$< 1.82 \times 10^{41}$		
1367	0.0214	11 42 29.5	19 53 02.0	4.84×10^{24}	NAT	11 42 28.8	19 53 13	1.97×10^{43}	130	50	0.01	119	1.46×10^{42}	32.3	0.003
1425	0.1120	11 55 45.8	26 37 53.8	3.63×10^{25}	CD		no detection	$< 2.11 \times 10^{42}$					$< 9.46 \times 10^{41}$		
1446	0.1028	11 59 31.2	58 18 50.0	1.66×10^{25}	WAT	11 59 32.5	58 19 26	3.91×10^{42}	10	135	0.07	359	1.65×10^{42}	16.7	0.001
1455	0.1390	12 01 03.4	28 13 32.9	9.81×10^{24}	WAT?		no detection	$< 1.94 \times 10^{42}$					$< 8.74 \times 10^{41}$		
1569	0.0784	12 33 37.4	16 54 57.6	7.81×10^{24}	TJ	12 33 38.8	16 55 11	1.93×10^{43}	30	0	0.03	74	1.80×10^{42}	4.3	0.0012
		12 33 55.1	16 48 47.5	1.66×10^{25}	WAT	12 34 02.2	16 49 11	1.93×10^{43}	20	110	0.15	72	9.12×10^{41}	3.9	0.0009
1589	0.0718	12 38 30.5	18 49 41.2	5.56×10^{24}	NAT	12 38 34.9	18 49 48	4.03×10^{43}	70	30	0.12	54	2.32×10^{42}	2.8	0.0025
1609	0.0891	12 43 54.8	26 43 39.4	5.76×10^{24}	TJ		no detection	$< 1.45 \times 10^{42}$					$< 6.52 \times 10^{41}$		
1656	0.0232	12 56 56.8	28 10 53.4	4.70×10^{23}	NAT	12 57 00.0	28 10 36	1.03×10^{44}	120	90	0.02	51	1.69×10^{41}	3.4	0.0036
1736	0.0461	13 24 00.2	-26 51 35.7	9.93×10^{23}	NAT	13 24 07.5	-26 54 50	6.50×10^{43}	110	50	0.18	121	5.26×10^{42}	cc	0.0052
	0.0461	13 24 26.8	-26 45 33.6	1.70×10^{23}	NAT	13 23 27.8	-27 11 13	6.50×10^{43}	110	160	0.52	121	5.26×10^{42}	cc	0.0052
1775	0.0724	13 39 31.0	26 37 18.8	3.02×10^{24}	NAT	13 39 33.3	26 37 13	8.27×10^{44}	145	30	0.04	130	3.42×10^{44}	cc	0.0082
1836	0.0365	13 59 01.7	-11 22 00.8	5.56×10^{24}	D	13 59 01.6	-11 22 01	3.54×10^{41}	40	40	0.01	73	3.23×10^{41}	2.8	0.0015
1890	0.0570	14 15 02.9	08 26 19.8	2.14×10^{24}	TJ	14 15 05.2	08 26 22	1.07×10^{43}	145	10	0.04	60	1.10×10^{42}	3.9	0.0020
1939	0.0883	14 35 00.6	24 58 31.1	2.77×10^{24}	TJ		no detection	$< 1.54 \times 10^{42}$					$< 6.91 \times 10^{41}$		
2022	0.0575	15 02 08.5	28 45 48.6	5.72×10^{24}	NAT	15 02 03.8	28 41 37	2.76×10^{41}		35	0.27	100	2.76×10^{41}	3.9	0.0004
2091	0.1333	15 31 54.8	10 26 45.8	1.94×10^{24}	TJ?		no detection	$< 4.59 \times 10^{42}$					$< 2.06 \times 10^{42}$		
2147	0.0354	16 00 18.4	15 53 35.9	2.09×10^{24}	Diff	16 00 20.8	15 53 12	1.88×10^{44}		55	0.03	76	2.54×10^{41}	3.8	0.0013
2162	0.0320	16 10 35.4	29 36 40.3	2.38×10^{23}	D	16 10 32.5	29 37 25	3.10×10^{42}	140	45	0.06	76	2.75×10^{41}	2.5	0.0016
2220	0.1106	16 38 24.4	53 52 30.0	1.54×10^{25}	WAT	16 38 31.7	53 51 54	6.59×10^{40}	60	65	0.02	133	5.30×10^{40}	7.6	0.0014
2256	0.0581	17 06 20.9	78 43 52.7	2.62×10^{23}	NAT	17 06 32.6	78 43 35	1.20×10^{44}			0.18	87	1.23×10^{43}	21.9	0.0037
2306	0.1271	18 26 23.3	74 42 05.8	3.65×10^{25}	WAT	18 26 30.9	74 42 60	4.13×10^{43}	40	20	0.32	113	1.05×10^{43}	cc	0.0021
2311	0.0899	18 49 47.3	70 17 33.7	2.68×10^{24}	NAT		no detection	$< 3.43 \times 10^{42}$					$< 1.55 \times 10^{41}$		
2634	0.0321	23 35 58.9	26 45 16.2	1.54×10^{25}	WAT	23 35 58.8	26 45 12	1.40×10^{42}	33	30	0.26	62	3.19×10^{41}	3.1	0.0023
		23 37 30.4	26 51 22.3	1.14×10^{24}	TJ	23 37 26.7	26 51 34	1.40×10^{42}	72	162		101	2.25×10^{41}	2.9	0.0048

* The clump X-ray luminosities listed for no detection clusters are 3 σ upper limits for a clump of radius 135".

** The letters "cc" in the last column indicate that the nearest significant peak in the X-ray is at the cluster center.

tion assuming the hydrogen column densities measured by Stark et al. (1992). Finally, the fluxes were converted to luminosities using the cluster redshifts and a Robertson-Walker cosmology. The uncertainties in the luminosities are estimated to be $\pm 30\%$ (Tananbaum et al. 1979).

X-ray fluxes and luminosities were also calculated for subclumps around radio galaxies (col. [13] in Table 1). The X-ray fluxes were computed for circular regions around the radio galaxies in a manner similar to that discussed above for the entire cluster. As noted in Table 1, the radius of the circle was typically 1.5–2′, comparable to the radio source size. These X-ray fluxes were also corrected for extended cluster emission by subtracting a local background from an annulus surrounding the circular region. The resulting clump luminosities reflect the X-ray environment in the immediate vicinity of the radio galaxy after correction for the larger scale ICM.

The significance of the X-ray peaks shown in Figure 1 is a crucial aspect of this work and merits special attention. We considered several different techniques for defining the substructure significance and finally settled upon what we believe is a simple and conservative method which we adapted from optical surface photometry. The significance of the X-ray peaks was judged by comparing the total X-ray count within a circle centered on a clump selected by eye with that in the background annulus which surrounds the X-ray peak. We chose the circles to be at least 1.5–2 times the FWHM diameter of the position-sensitive proportional counter (PSPC) beam. The background annulus (typically with a width of 2′) was carefully selected to avoid nearby substructure but to include any diffuse cluster gas emission. The signal-to-noise ratio was then computed, assuming Poisson statistics, and this ratio is listed in Table 1 (col. [15]).

Position angles of the X-ray emission were determined using the program ELLIPSE running under STSDAS in the IRAF environment. This program fits elliptical isophotes as a function of distance from the X-ray centroid. The algorithm has been described by Jedrzejewski (1987). The X-ray position angle listed in Table 1, θ_x, is that measured near the extremities of the radio source.

The radio source position angle, θ_r, is somewhat more difficult to define. We chose to measure θ_r as the position angle of the line that passes through the optical galaxy and bisects the radio source. For WAT and NAT sources, this is the position angle of the line drawn between the galaxy's optical position and the midpoint between the radio tails. For more linear sources with jets, this angle is approximately perpendicular to the line drawn between the radio lobes or perpendicular to the jets. These angles were measured by eye from the radio maps.

Finally, we note that three positions are used for our analyses of these clusters. The first is the optical position of the cluster center taken from Abell, Corwin, & Olowin (1989). The rms errors in the cluster center positions are estimated to be 3.2 in right ascension and 2.4 in declination (Abell et al. 1989). The second is the position of the radio source; we took this to be the location of the optically identified radio galaxy, since radio cores were not seen for all the radio sources at the VLA survey resolution. This position is accurate to $\approx 1''$. The third is the position of the X-ray emission, which was taken to be the location of the nearest statistically significant X-ray peak. The accuracy of the X-ray peak position is typically $\approx 20''$, although this depends on the strength of the X-ray peak (Harris et al. 1990).

2.2. *X-Ray/Radio Overlays*

To compare the radio and X-ray images, we first rescaled and repositioned the *Einstein* images to match the VLA maps. Subsections of the IPC images were interpolated onto new grids which contained the same pixel size, field of view, and image center as the VLA maps using the AIPS task HGEOM. Gray-scale images of the radio emission were then overlaid onto contours of the X-ray surface brightness. The first X-ray contour was generally taken to be twice the rms noise measured off of the cluster emission, except for the very bright clusters, where a more appropriate, larger value for the first contour was chosen. These X-ray/radio overlays are displayed in Figure 1. The crosses in Figure 1 represent the positions of the Abell cluster centers where the size of the crosses is equal the rms errors in the cluster center positions as discussed above. For images without crosses, the Abell centers lie outside the image boundaries.

Detailed comments on the X-ray, radio, and optical properties of the individual clusters are given in the Appendix.

3. DISCUSSION

3.1. *General Impressions from the X-Ray/Radio Overlays*

Upon inspection of the overlays in Figure 1, several features are immediately obvious. First, the spatial distribution of X-ray emission in most of the clusters in our sample is irregular and clumpy. Prominent X-ray substructure is present in numerous clusters such as A98, A160, A514, A1367, A1569, A1589, A1656, A2147, and A2306. This substructure includes individual clumps (many of which are significant according to our criterion in § 2.1) such as those in A1569 and "extensions" of X-ray emission as in A2147. Forman & Jones (1990 and references therein) state that there is X-ray substructure in $\approx 30\%$ of the clusters from the *Einstein* database. However, Mohr, Fabricant, & Geller (1993) suggest that $\geq 68\%$ of $z < 0.06$ Abell clusters with good detections in the *Einstein* database have evidence of X-ray substructure as a result of their analysis of the moments of the X-ray surface brightness. In our sample of radio-loud clusters, we find that $26/36 = 72\%$ of the clusters have multiple X-ray components, where the X-ray clumps have surface brightness that are more than 3 times the surrounding emission. So it appears that the clusters in Table 1 have a comparable amount of substructure to that claimed by Mohr et al. (1993) for Abell clusters as a whole; but the new aspect of this clumping is that X-ray substructure is often found around radio galaxies that lie within the clusters. Clusters with substructure in our sample are consistent with "early" or unevolved systems in the Forman & Jones (1982) X-ray cluster classification scheme. Clusters without clear substructure are generally ones that contain a single central dominant galaxy (e.g., A133, A401, A780, A1446), have centrally peaked X-ray emission (classified XD by Forman & Jones 1983), and may possess cooling inflows (e.g., Fabian, Nulsen, & Canizares 1991; Burns 1990).

Second, the X-ray structure is sometimes, but not always, correlated with optical clumping of galaxies within the clusters. We have inspected the Palomar Sky Survey E prints in and around the locations of prominent X-ray subclumps in our sample clusters. Notes on our visual impressions are given in the Appendix. In cases such as A98, A1569, A1589, and A2306, galaxy subclusters appear to trace the substructure in the X-ray. However, in cases such as A514 the galaxies do not seem

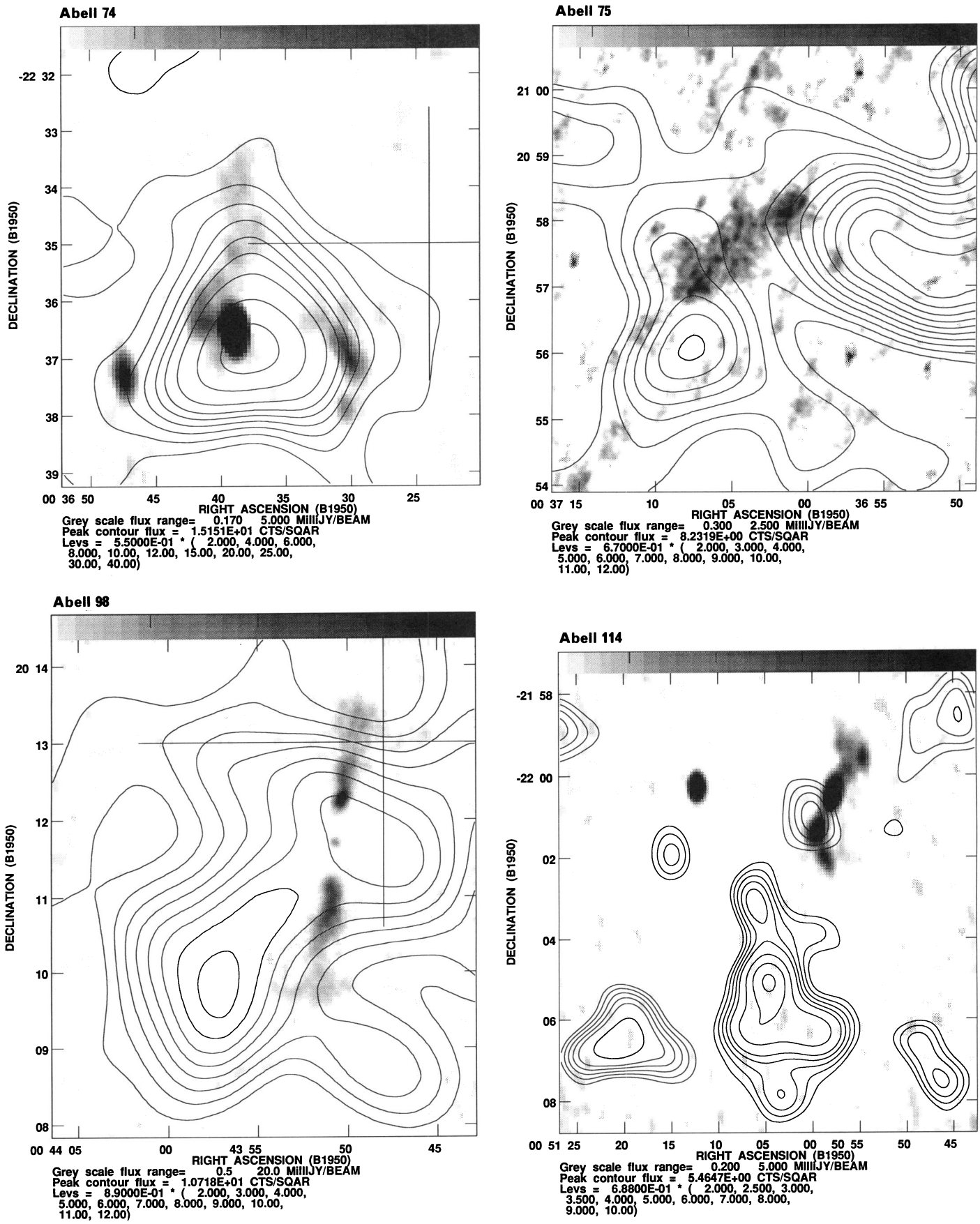

FIG. 1.—Overlays of 20 cm radio emission (gray scale) onto contours of X-ray surface brightness. The cross marks the position of the Abell cluster center (Abell et al. 1989), and the cross size reflects the estimated average error in that position.

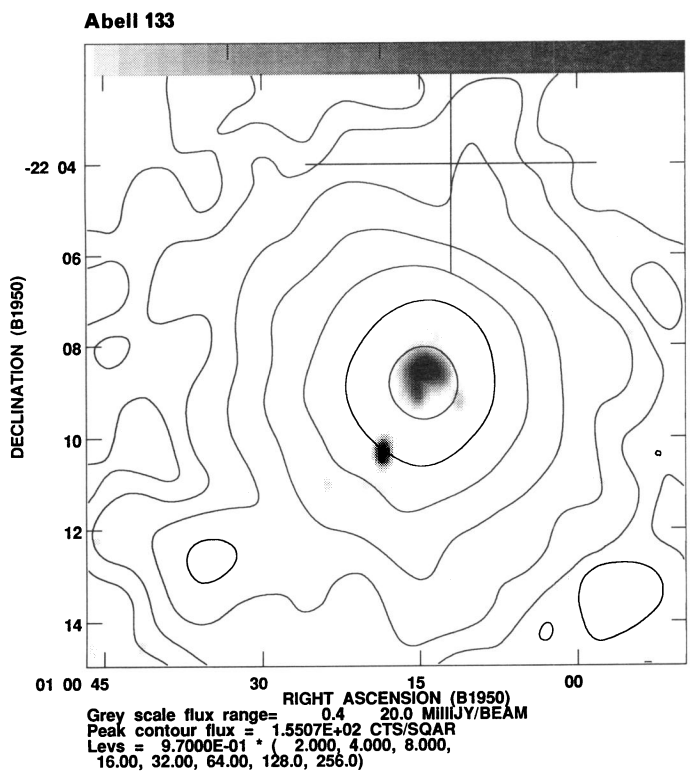

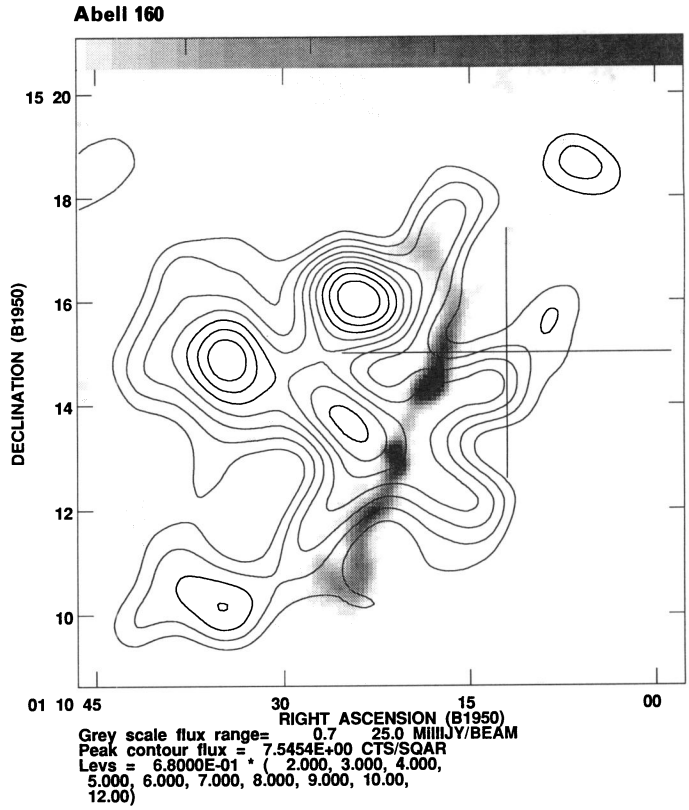

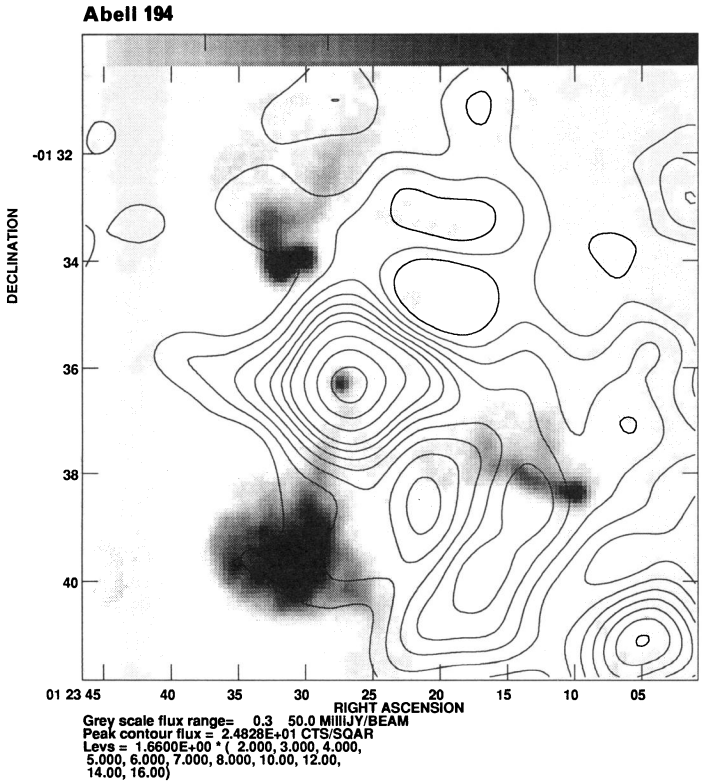

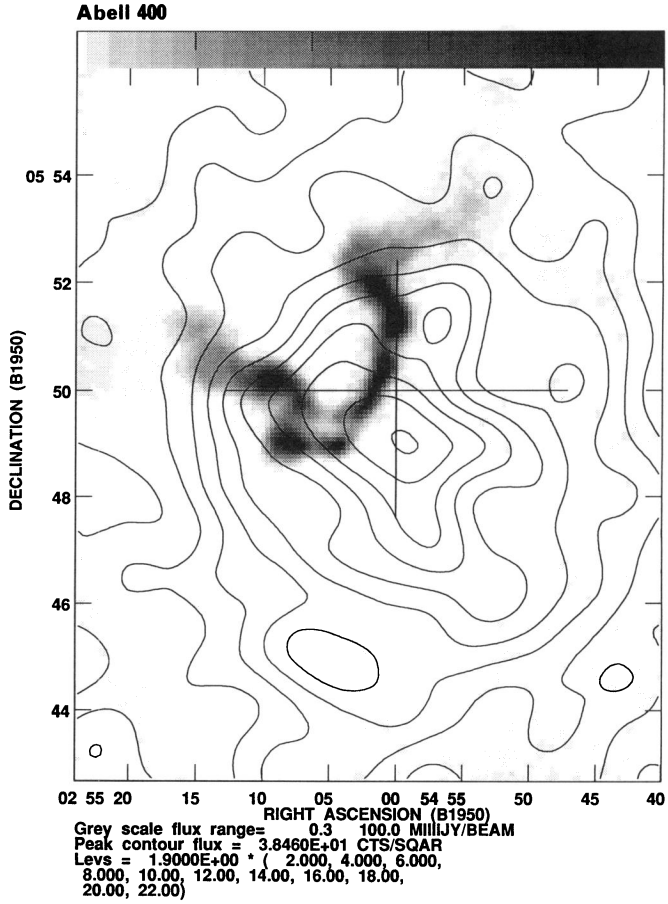

FIG. 1—*Continued*

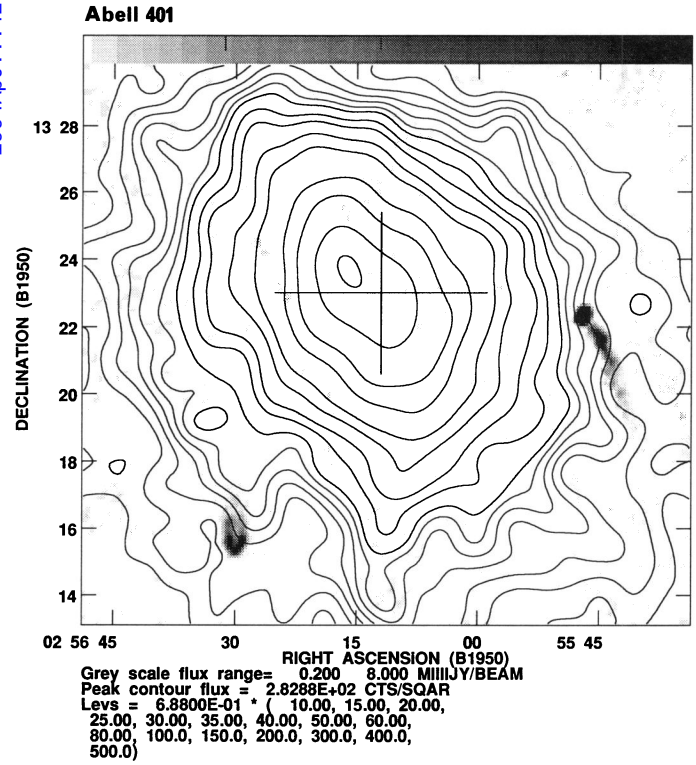

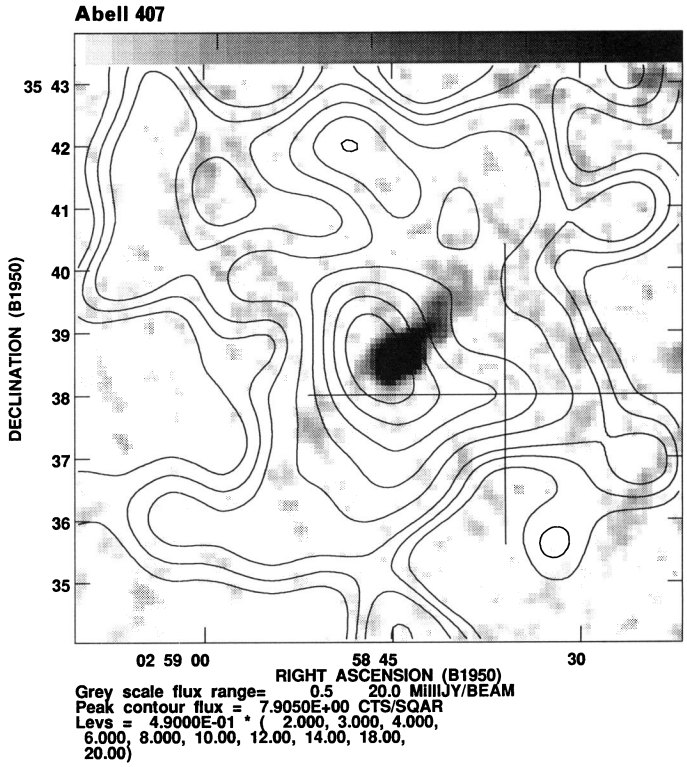

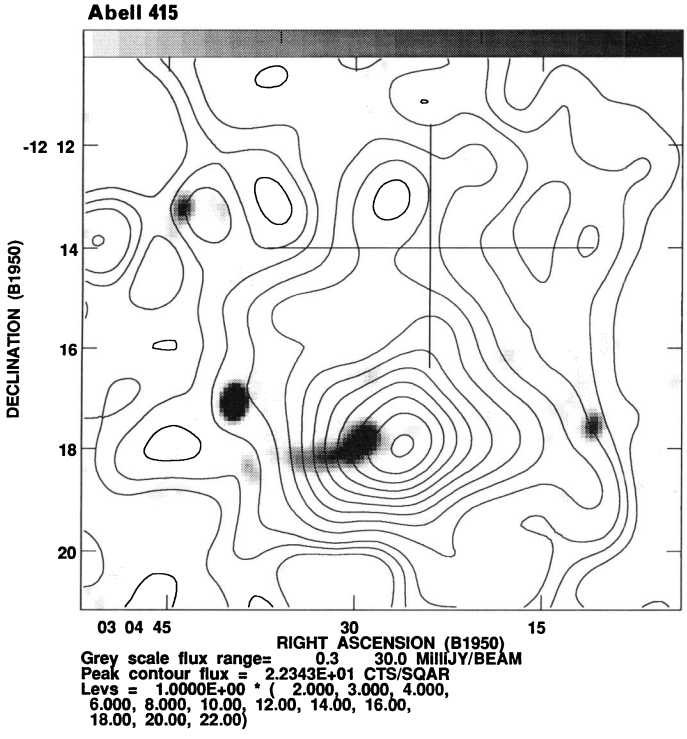

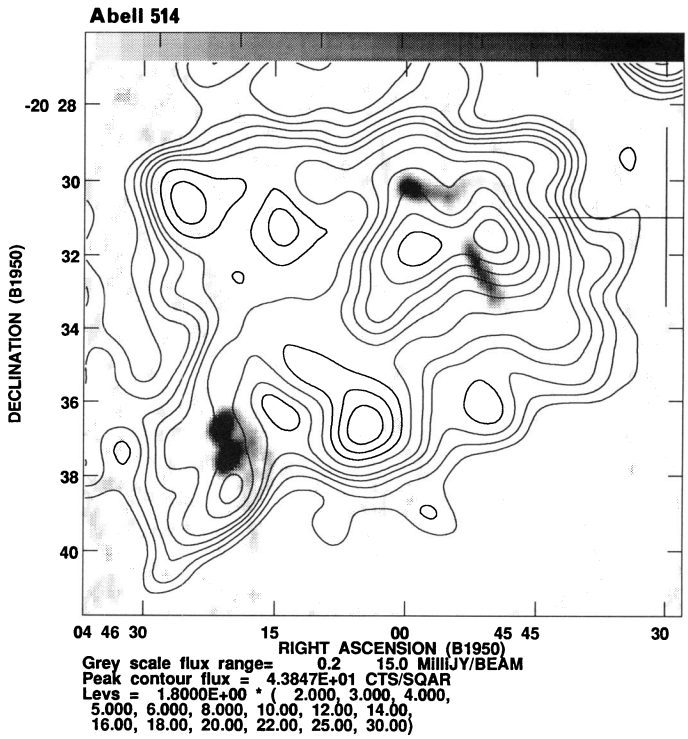

FIG. 1—*Continued*

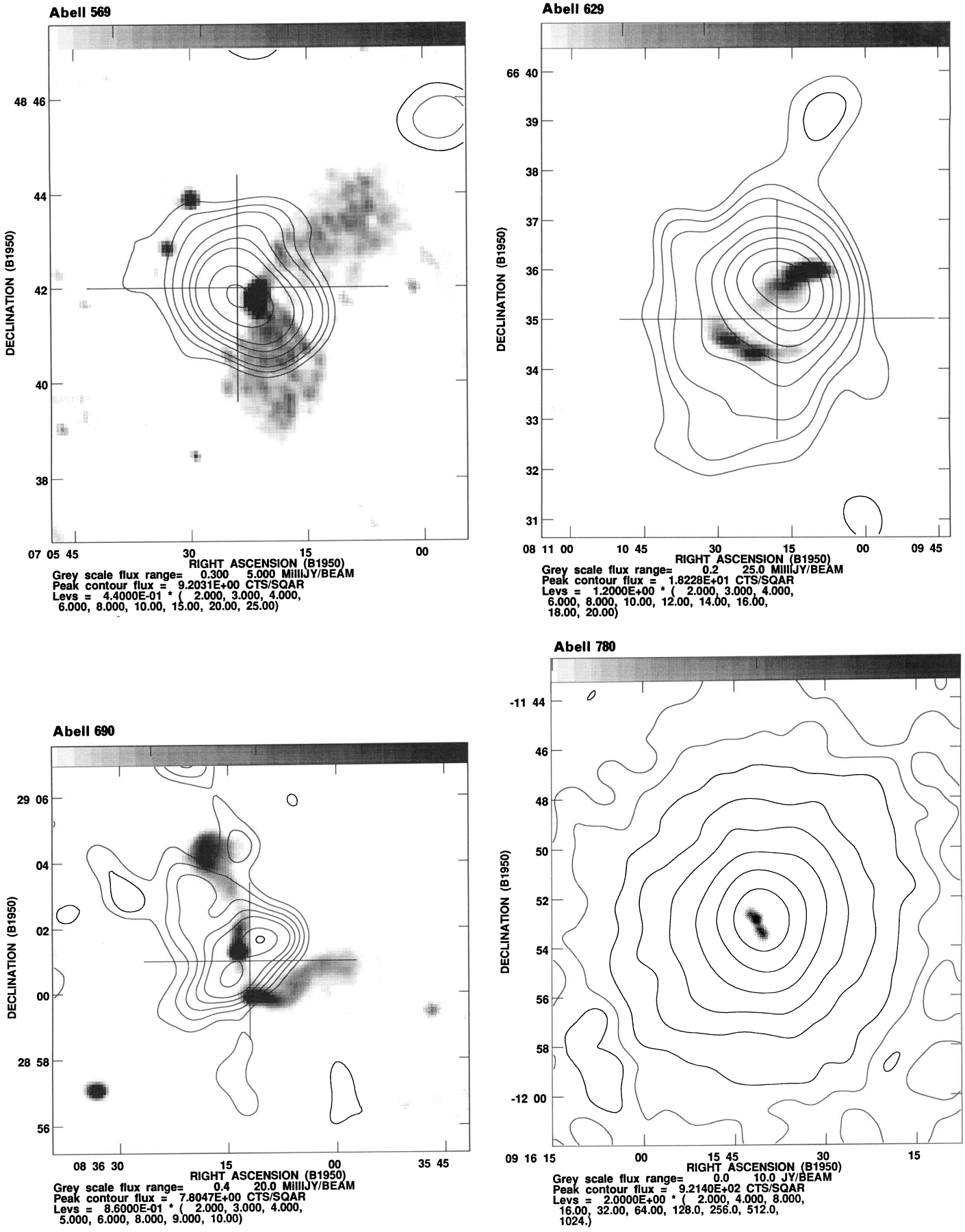

FIG. 1—*Continued*

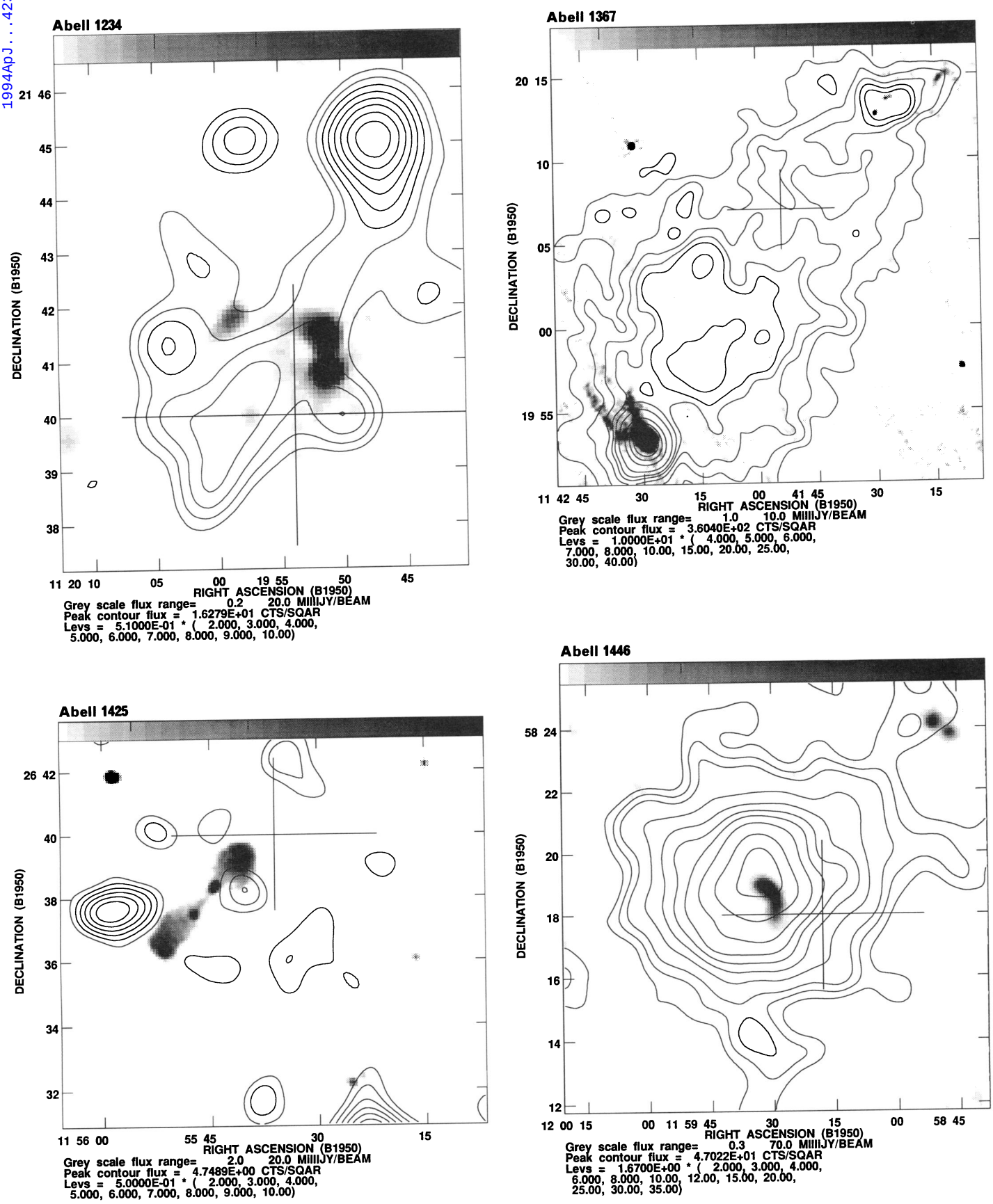

FIG. 1—*Continued*

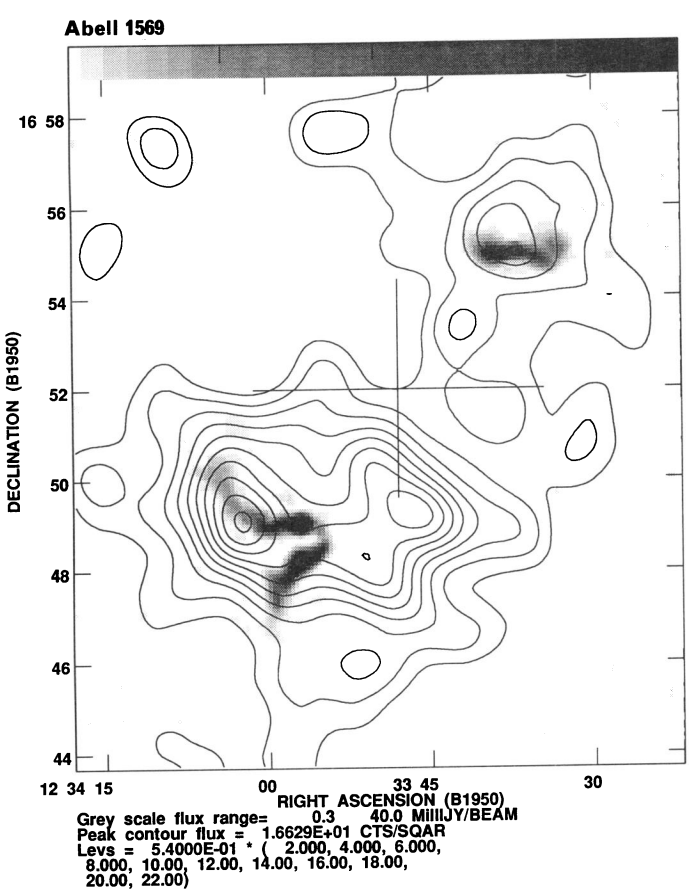

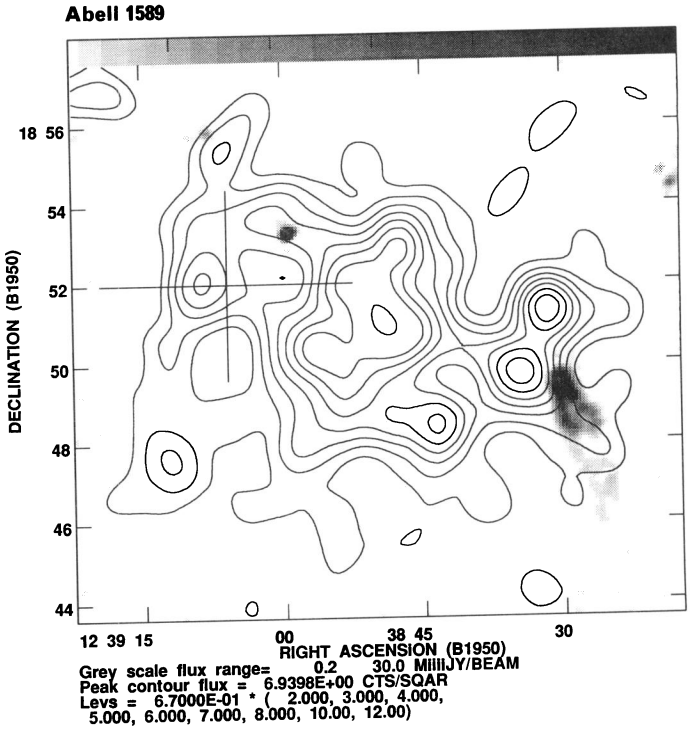

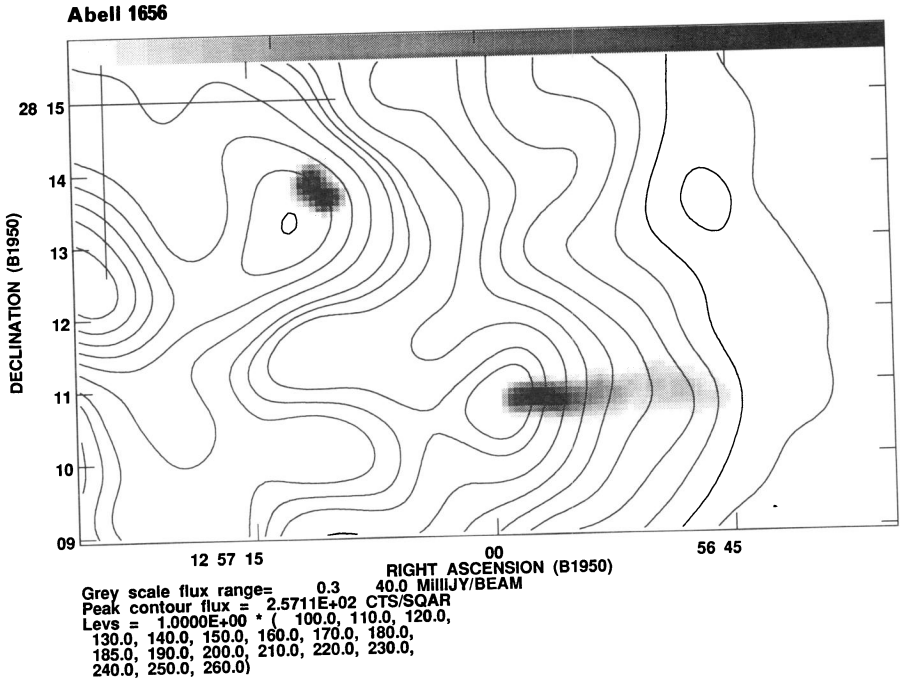

FIG. 1—*Continued*

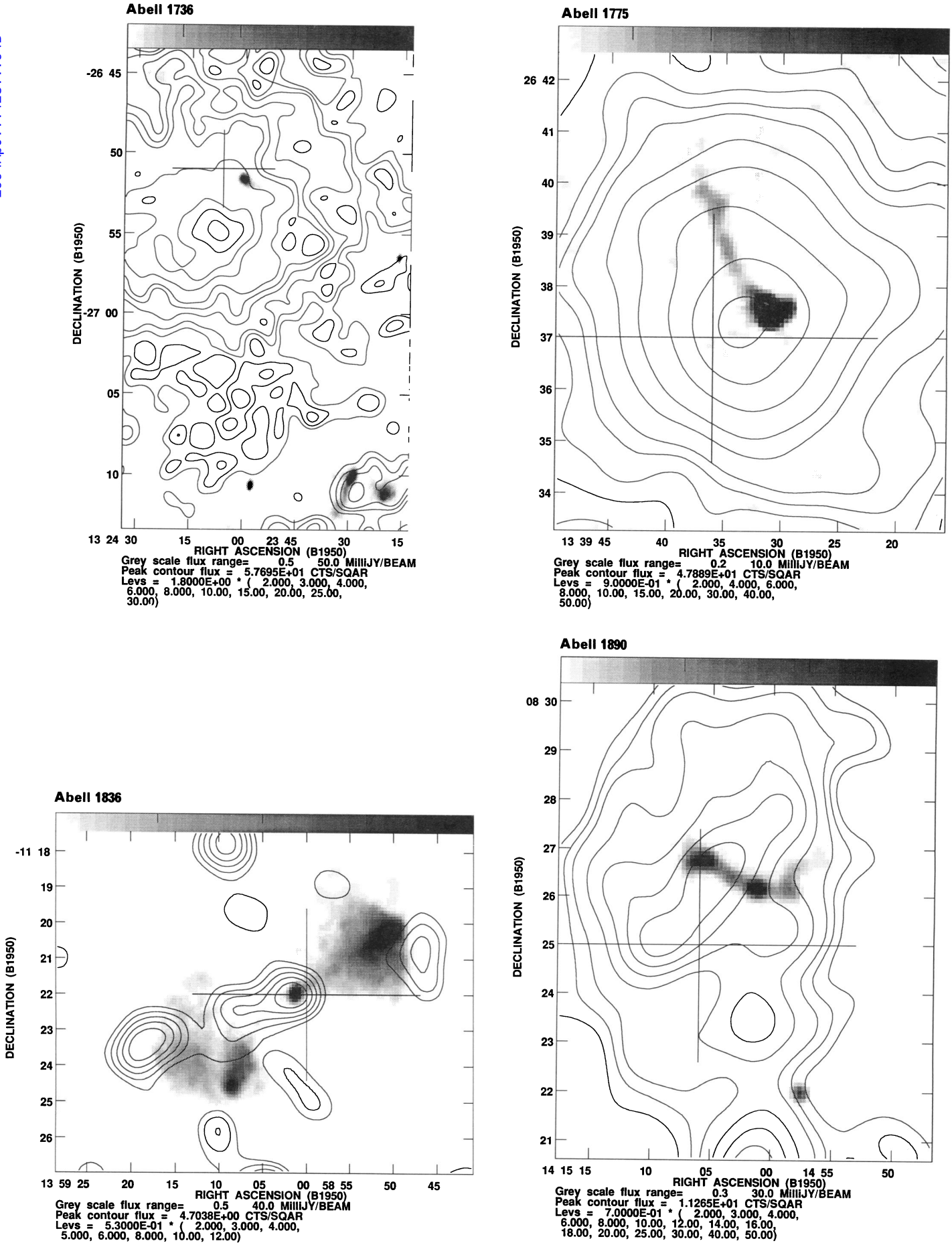

FIG. 1—*Continued*

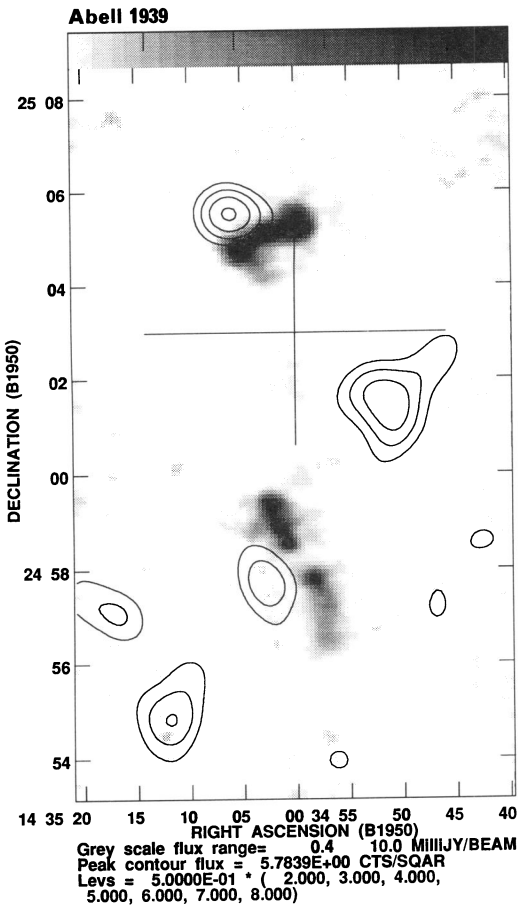

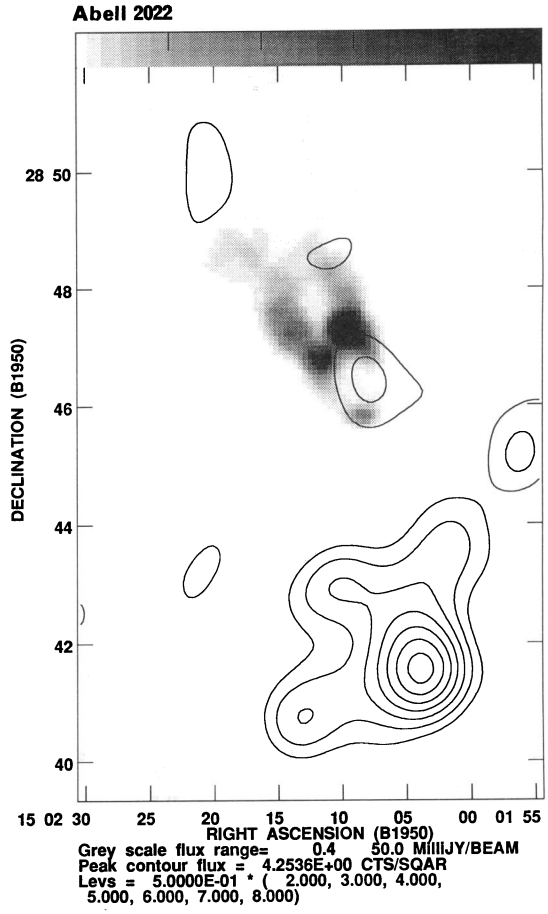

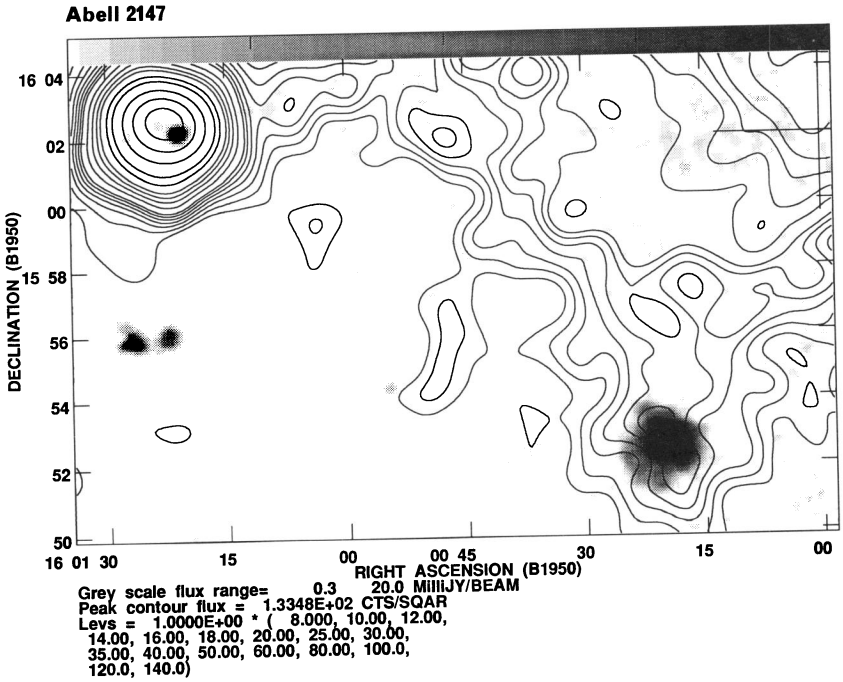

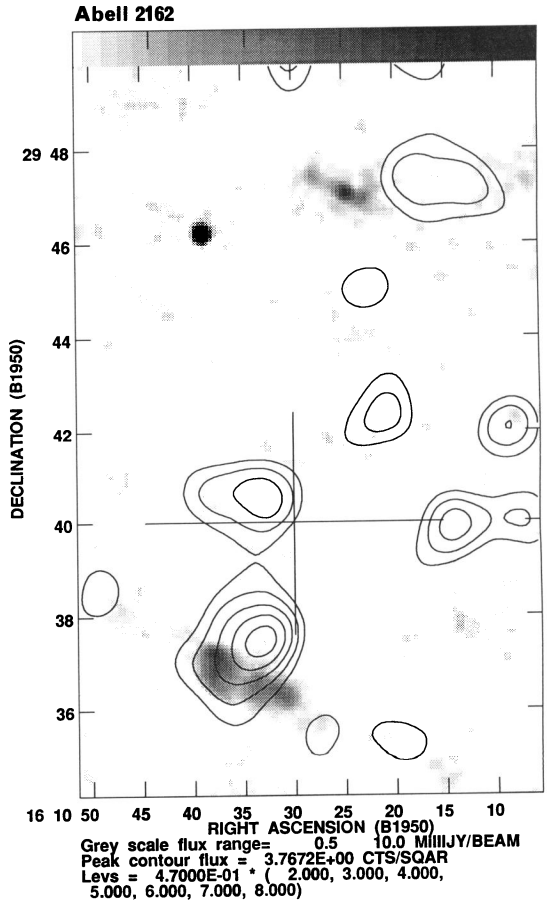

FIG. 1—*Continued*

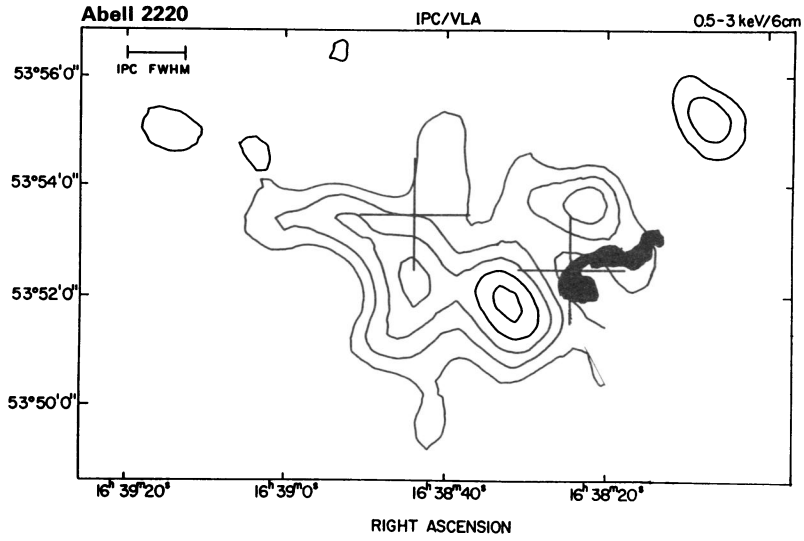

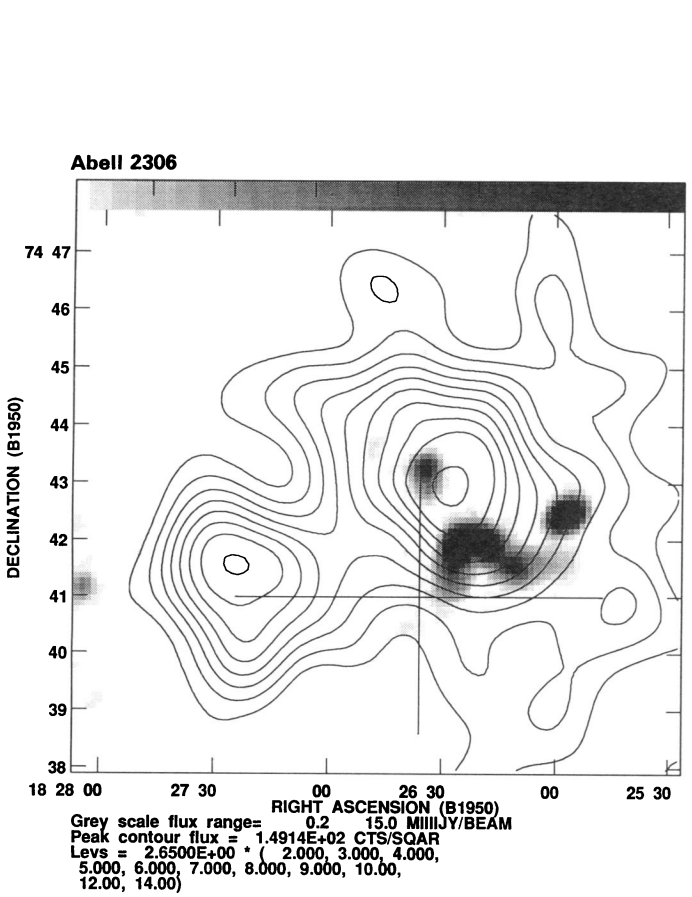

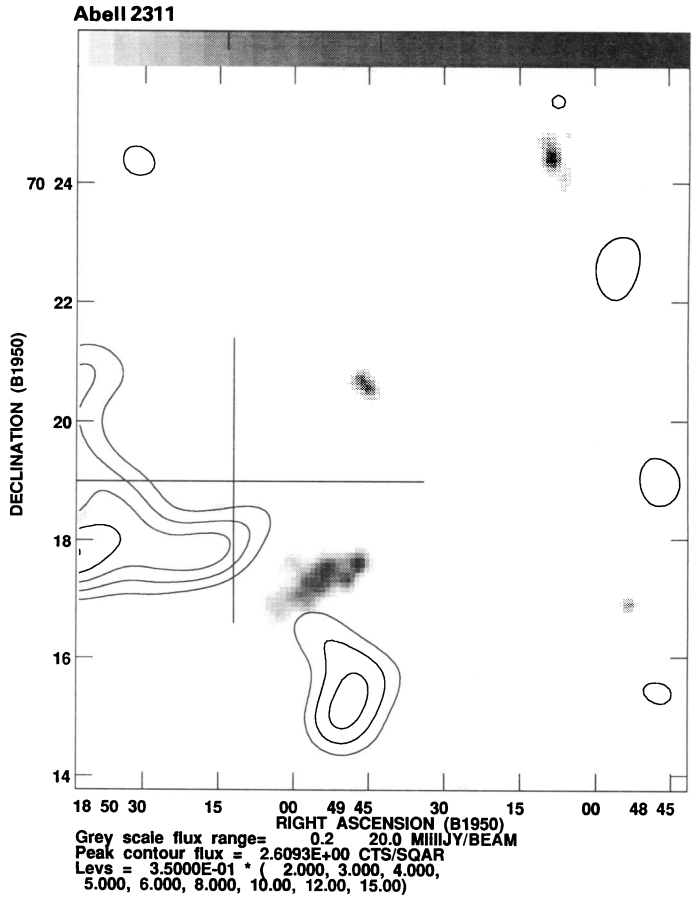

FIG. 1—*Continued*

to follow the X-ray substructure. For A1367 and A1656 the radio galaxies alone appear to coincide with compact, high surface brightness X-ray peaks.

Third, there is a strong tendency for radio galaxies to coincide with peaks in the X-ray emission. Not every X-ray peak contains a radio galaxy, but there appears to be a high probability that radio galaxies are found near X-ray peaks. This spatial coincidence is obviously true for radio-loud centrally dominant galaxies such as those in A133, A400, A569, A780, A1446, and A2634. However, most of the radio galaxies are not associated with dominant galaxies and yet many occur close to X-ray subclumps such as in A114, A514, A1367, A1569, A1589,

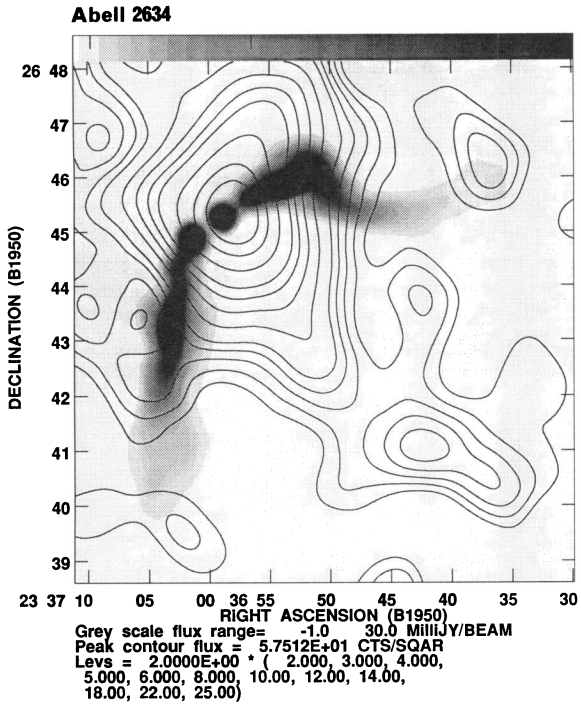

FIG. 1—*Continued*

A1656, A2022, and A2147. The statistics of this association will be described further in the next section.

Fourth, there are a few linear, double-lobed radio sources in our sample in Table 1. Because of the small number, we have included all sources which have evidence of radio lobes and are roughly linear (i.e., both Fanaroff-Riley 1974 classes I and II) in what follows. Interestingly, we find that in such clusters as A1425, A1836, A1939, and A2162 there is little or no detected X-ray emission around the double-lobe radio galaxies or in the clusters. These radio galaxies appear to dwell in rather poor gaseous environments even though they are within Abell clusters. Brown & Burns (1991) also noted that classical doubles from the Parkes survey which are identified with cluster galaxies (i.e., consistent in redshift) tend to occur in the outer, presumably gas-poor portions of southern rich clusters. We will pursue this interesting topic again in a later paper with a larger sample using the *ROSAT* all-sky survey.

3.2. *Statistics of X-Ray/Radio Coincidences*

The distributions of radio galaxy positions with respect to the nearest significant X-ray peaks and with respect to the Abell cluster centers are shown in Figure 2. The separation distances in these histograms are in units of corrected Abell radii.

It is clear from these figures that radio galaxies are tightly correlated with the centers of Abell clusters but even more strongly correlated with peaks in the cluster X-ray surface brightness distributions. There are 34 radio sources out of our sample of 52, or 65%, located within 5′ of the Abell cluster center, and 4 out of 52, or 7%, located within 1′. However, there are 39 radio galaxies out of 52, or 75%, that are within 5′ of a statistically significant X-ray peak, and 24 out of 52, or 46%, within 1′. One factor that might contribute to the somewhat poorer correlation of radio galaxies with Abell cluster centers relative to the X-ray/radio correlation is the considerably larger uncertainties in the Abell center positions as discussed in § 2.1.

We have made a simple test to compare the radio galaxy and X-ray clump distributions with that of a King model (Fig. 2*a*). For an isothermal cluster in hydrostatic equilibrium, the projected surface density of galaxies is expected to follow (e.g., Binney & Tremaine 1987, p. 230)

$$\rho = \rho_0[1 + (R/R_c)^2]^{-1}\,, \qquad (1)$$

within several core radii (R_c, which we take to be 250 kpc, the average value for a large number of Abell clusters studied by Rhee, van Haarlem, & Katgert 1991a). This distribution is plotted as a dashed histogram in Figure 2*a*. If the radio galaxies were distributed as are other galaxies in clusters (i.e., a King model), we would expect twice as many galaxies in the range 0–to 0.2 R_c as in the range 0.2–0.3 R_c. For our sample in Table 1, however, the ratio of radio galaxies in the interval 0–0.2 R_c from the Abell cluster center to that in the interval 0.2–0.3 R_c is 6.2. For the distribution of distances between radio galaxy positions and X-ray clump centers in Figure 2*b*, this ratio is 19.6.

A χ^2 test was also run on the separation distributions in Figure 2 (radio/Abell and radio/X-ray) as contrasted with the above King model. We find that the probability that the radio/Abell distribution is drawn from a King model with $R_c = 250$ kpc is 1.6%. A similar comparison for the radio/X-ray distribution indicates a probability of less than 10^{-7}. We also varied R_c for the King model between 10 and 300 kpc and performed the same χ^2 test; we found no significant differences in the probabilities. It is not yet clear whether the narrow distribution in Figure 2*b* means that the radio/X-ray distribution is intrinsically narrow or that radio galaxies preferentially lie in X-ray clumps.

Finally, we ask whether the observed radio/X-ray distribution is significantly different from that expected by random chance. To address this question, we performed a series of 1000 Monte Carlo simulations in which radio galaxy positions were compared with those of X-ray clumps which follow a King model profile but are otherwise randomly placed within the cluster. We chose to put two X-ray clumps in each cluster, which appears to be the average number seen in Figure 1. The resulting distribution is shown in Figure 2*b*. The χ^2 probability that the two distributions in Figure 2*b* are drawn from the same parent population is 0.4%.

For completeness, we show the distribution of projected separations between the Abell cluster centers and the X-ray peaks in Figure 2*c*.

We conclude that radio galaxies are more strongly correlated with cluster centers than other radio-quiet galaxies in the clusters. But, more important, the distribution of projected distances of radio galaxies from X-ray clumps is even more strongly peaked and does not seem to follow a standard King model distribution.

3.3. *What Produces the Radio/X-Ray Correlation?*

The obvious question is, What is the origin of the correlation between the radio galaxy and X-ray peak positions? One possible explanation is that the gravitational potential well of many clusters is intrinsically clumpy (possibly resulting from cluster mergers). If both the gas and the galaxies (including the radio galaxies) follow the potential well, then this would suggest an indirect relationship between the X-ray and radio emissions. Although there is indeed evidence that galaxies do

follow the X-ray clumps in many clusters, there are examples described in the Appendix where X-ray peaks are much stronger than galaxy peaks, or X-ray extensions do not correlate with the galaxy distribution. Thus, other factors may play an important role in determining the radio/X-ray correlation.

It is generally acceptable that the extended radio emission coming from active galaxies is produced by incoherent synchrotron radiation generated by a population of nonthermal electrons spiraling in a magnetic field (e.g., Pacholczyk 1970). For a correlation to occur between the X-ray and radio emissions, there may be a direct link between the mechanisms producing the radiation at the two different wave bands and/or an interaction between the plasmas radiating at the two wave bands. We now consider three different mechanisms for the production of the X-ray emission which might lead to the observed correlations.

First, the general intracluster medium is hot (10^7–10^8 K) and relatively dense ($n \approx 10^{-3}$ cm^{-3}). It radiates free-free plus line emission in the X-ray (e.g., Sarazin 1986). Given this preponderance of hot gas between galaxies in clusters, might the observed peaks of X-ray emission around the radio galaxies simply be clumps of slightly denser gas? The X-ray and radio emission properties could be correlated if the pressure from the X-ray clumps is responsible for confining the radio plasma. For extended, relaxed radio structures such as tails in NATs and WATs, the confinement pressure is simply nkT. This can be rewritten in terms of the X-ray free-free luminosity between photon energies $E_1 = 0.3$ keV and $E_2 = 4.5$ keV (the *Einstein*

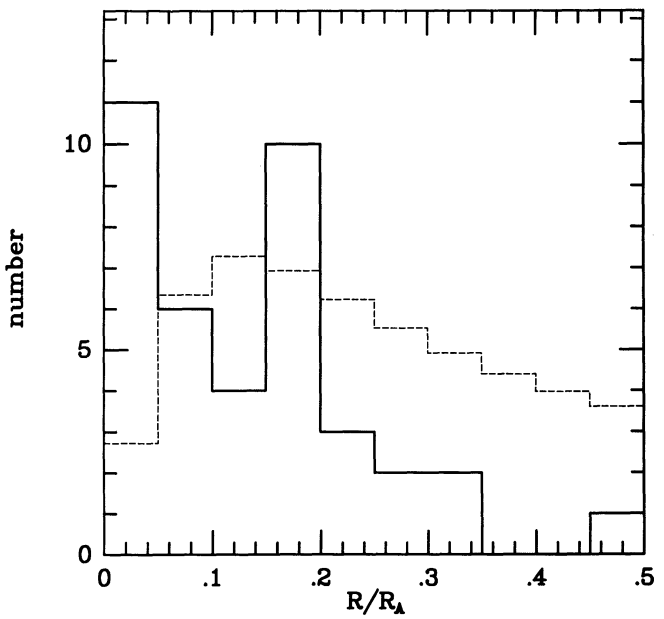

FIG. 2a

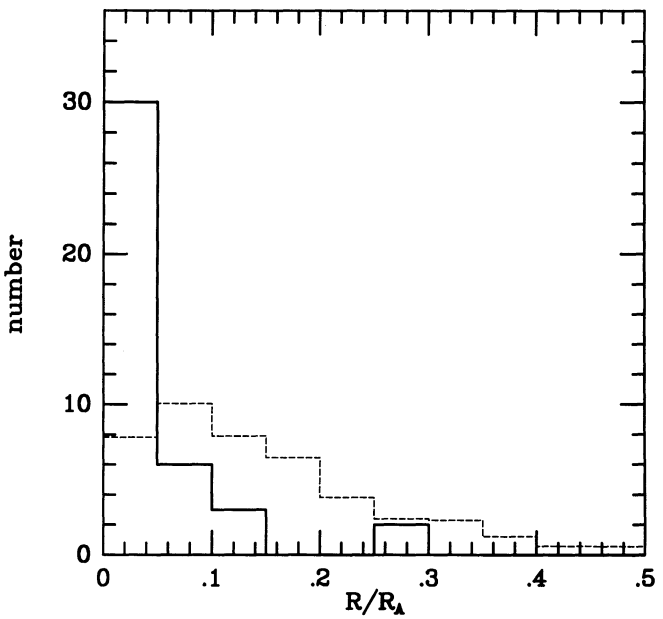

FIG. 2b

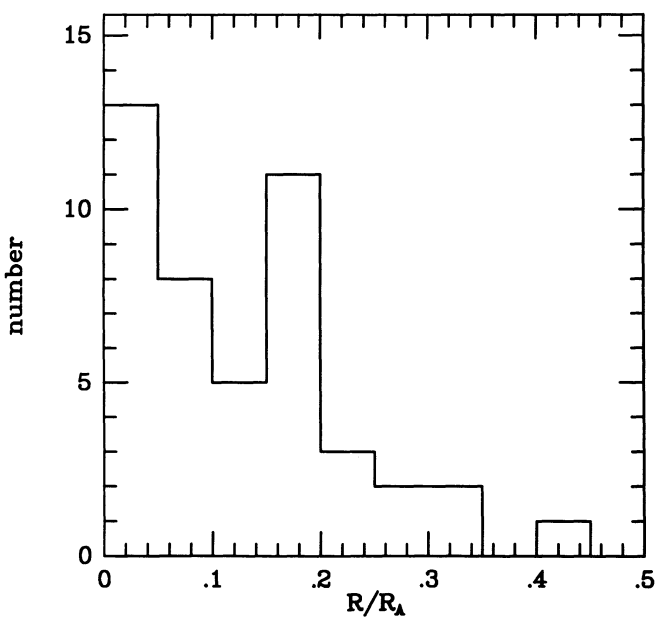

FIG. 2c

FIG. 2.—(*a*) Distribution of separation distances between radio galaxies and Abell cluster centers. The distances are in units of Abell cluster radii ($R_A = 2$ Mpc for $H_0 = 75$ km s^{-1} Mpc^{-1}). The dashed histogram shows the prediction for a King model with a core radius of 250 kpc. (*b*) Distribution of separation distances between radio galaxies and the nearest X-ray peak using the same units as in (*a*). The dashed histogram is the result of 1000 Monte Carlo simulations assuming that an average of two X-ray clumps per cluster are randomly placed with respect to the radio galaxy. (*c*) Distribution of separation distances between the X-ray clumps closest to the radio galaxies and the Abell cluster centers.

bandpass) for a spherical gas clump with temperature T, density n, and radius $R_{\rm clump}$ given by (e.g., Tucker 1975)

$$L_X = 8.4 \times 10^{-27} g n^2 R_{\rm clump}^3 T^{0.5} (e^{-E_1/kT} - e^{-E_2/kT}) \text{ ergs s}^{-1} , \quad (2)$$

where g is the Gaunt factor (≈ 1.2). Using equation (2), we have estimated the average density of gas in each X-ray subclump assuming $T = 3$ keV; these values are listed in Table 1. Also from equation (2), we see that $nkT \propto L_X^{0.5} T^{0.75} R_{\rm clump}^{-1.5}$. Furthermore, if the relativistic particles and magnetic fields in the radio source are in energy equipartition, it can be shown that the internal radio plasma pressure is proportional to $P_R^{4/7}$, where P_R is the radio power (e.g., Pacholczyk 1970). Thus, one might expect that $P_R \propto L_X^{0.9} T^{1.3} R_{\rm clump}^{-2.6}$ if the radio plasma is thermally confined by the clumped X-ray gas.

Second, an alternative origin for the X-ray peaks could be nonthermal emission from the active galactic nuclei (AGNs), which are also responsible for the generation of the radio emission. Such X-ray emission is compact and may be relatively high surface brightness. There are some good candidates in our sample for such compact X-ray emissions which coincide with the radio galaxy cores (e.g., A194, A415, A1367, A1656). For a sample of 40 3CR radio galaxies observed by *Einstein*, Fabbiano et al. (1984) detected 26 (65%) and found a correlation between X-ray luminosity and radio power such that $L_X \propto P_R^{0.72 \pm 0.15}$. Fabbiano et al. proposed that this correlation could best be explained if the X-ray emission originated from AGNs. However, many of their radio galaxies lie in rich and poor clusters, and it is not clear whether they successfully isolated all the cluster emission from the purported AGN emission using a circle with 2′ radius. In contrast, for a smaller sample of 18 3CR radio galaxies, Feigelson & Berg (1983) proposed that most of the X-ray emission has its origin from cluster gas. Similarly, Morganti et al. (1988) examined *Einstein* images for 22 B2 radio sources (45% of which were in Abell clusters) and concluded that the extended radio plasma appeared to be in pressure equilibrium with the surrounding gas, assuming that the X-ray emission is produced by free-free radiation.

Recently, Crawford, & Fabian (1993) claimed that the marginally extended X-ray emission around 3C 356 observed by *ROSAT* is caused by hot gas possibly in a cooling inflow. Also, Birkinshaw & Worrall (1993) reported that the *ROSAT* X-ray spectrum and image of the radio galaxy NGC 6251 (associated with a Mpc-sized radio source) suggested a two-component model—a 0.5 keV temperature slightly extended thermal gas and a pointlike harder component, which collectively may be within a cooling inflow. Furthermore, from *ROSAT* X-ray spectra of two radio galaxies in the Perseus cluster, Rhee, Burns, & Kowalski (1994) find that the compact X-ray emission around IC 310 (a NAT) is best fitted by a power-law spectrum, whereas the X-ray spectrum of a second cluster radio galaxy with more diffuse X-ray emission around it is best fitted by a Raymond-Smith model. Thus, there is evidence that both hot gas and AGNs may be responsible for some of the X-ray emission near radio galaxies in clusters. The situation will remain unclear until X-ray spectra are available for many more of the radio galaxies and their surrounding clusters in Figure 1.

Third, inverse Compton (IC) scattering of the microwave background photons off the relativistic electrons in extended radio sources should produce X-ray radiation at some level. The electron energies [$\gamma = E_e/(m_e c^2)$] required to boost the microwave photons to X-ray energies, $\gamma = E_X/(3.6kT) = 1500$ for $E_X = 2$ keV, are lower than that needed to produce the synchrotron radiation at 20 cm,

$$\gamma = 4255[\nu/(1450 \text{ MHz})]^{0.5} [B/(10\ \mu\text{G})]^{-0.5} .$$

Following Daly's (1992) approach, the ratio of the IC X-ray flux density to that of the radio flux density is

$$\frac{S_{\rm IC}}{S_R} = 5.3 \times 10^{-13} \left(\frac{B}{10\ \mu\text{G}}\right)^{-(1+\alpha)} X(\alpha) \left(\frac{1 \text{ keV}}{E_X} \frac{\nu_R}{178 \text{ MHz}}\right)^{\alpha} , \quad (3)$$

where α is the spectral index ($S_R \propto \nu^{-\alpha}$), and $X(\alpha)$ is a combination of variables whose value is 80 for $\alpha = 0.7$ and 160 for $\alpha = 1.0$. This ratio in equation (3) equals 1.16×10^{-10} for $\alpha = 0.7$. For $S_R(20 \text{ cm}) = 0.5$ Jy and $z = 0.05$ (typical of the sources in Table 1), and integrating over the *Einstein* bandpass, we find that the predicted IC X-ray luminosity is 3×10^{39} ergs s^{-1}. This is about a factor of 100 lower than the observed X-ray luminosities of the subclumps/peaks around the radio galaxies. Daly also suggests that some inverse Compton emission can be produced by a "postlobe" (i.e., an expanded plasma around the observed radio source where the relativistic electrons have adiabatically cooled to the point where their energy loss is dominated by IC rather than synchrotron emission). However, for the parameters used above, we find that this postlobe IC emission does not substantially add to the observed X-ray emission. Thus, it appears that IC emission is not likely to be the dominant source of X-ray emission around these cluster radio galaxies.

In summary, it would appear that a combination of clumped hot gas and some AGN emission likely contributes to the spatial X-ray/radio correlations that we observe around radio galaxies in clusters. Compact, high surface brightness X-ray emissions coincident with radio galaxy cores are good candidates for AGNs, whereas extended, diffuse X-ray emission around the radio galaxy is good evidence for free-free radiation from hot gas. X-ray spectra of these clumps would definitively differentiate between the above radiation processes. For many of the clusters in Table 1, it appears that the underlying gravitational potential well is itself clumped, which produces an alignment of X-ray emission and galaxy distributions within the clusters.

3.4. *Further Comparisons of X-Ray and Radio Properties*

In addition to the excellent spatial coincidences between radio galaxies and X-ray peaks, do the radio and X-ray luminosities correlate for these clusters? In Figure 3*a* we show a plot of the 20 cm radio power versus the isophotal cluster X-ray luminosities from Table 1. We used the survival analysis statistical package ASURV (Isobe & Feigelson 1990; Feigelson & Nelson 1985), which allows upper limits, to investigate any correlation between these variables. The generalized Kendall's τ-test indicates the probability that a correlation is not present is 40%, and Spearman's ρ-test similarly indicates a probability of 30%. Thus, there does not appear to be a significant correlation between the radio power and the total X-ray luminosity. This agrees with the results of Zhao et al. (1989) in Paper I for a somewhat different subsample of Abell clusters.

We also asked whether there was a relationship between the radio power and the X-ray luminosity of the peaks or subclumps nearest the radio galaxies. Since there is no correlation with the global cluster X-ray properties, might there be a more

local effect? It is interesting to note that the X-ray subclump luminosities are comparable to those measured for individual elliptical galaxies, 10^{38}–10^{42} ergs s^{-1} (Fabiano 1989). We show a plot of P_{20} versus $L_{X\ \mathrm{clump}}$ in Figure 3*b*. We again ran the ASURV software to investigate any potential correlation. The probability that a correlation is not present is 0.1% according to the generalized Kendall's τ-test and 0.4% according to Spearman's ρ-test. Using Schmitt's linear regression method, the best-fit line to these data suggests that $P_{20} \propto L_{X\ \mathrm{clump}}^{0.8 \pm 0.2}$, where the quoted error is 1 σ.

Although the above is somewhat consistent with the expectations from the free-free plus thermal confinement model in § 3.3, serious consideration must be given to possible selection effects. We find that when the X-ray clump luminosities are normalized to a constant linear aperture size, the above correlation disappears. Furthermore, although there is no correlation between radio power and redshift, we find a strong correlation between L_X and z. Thus, we are concerned that the radio/X-ray clump luminosity relation may be an artifact of the sample selection and the limited X-ray resolution.

We also examined the relationship between radio power and X-ray clump size as predicted by the free-free model in § 3.3. Here, too, there appears to be a correlation, as shown in Figure 3*c*. Kendall's τ-test and Spearman's ρ-test indicate that this relationship is consistent with the null hypothesis at the 0.01% and 0.04% levels, respectively. However, the power-law index for this correlation in Figure 3*c* is 0.26 $\pm$ 0.09, which is completely inconsistent with the prediction in § 3.3. Once again, we also find a strong correlation between X-ray clump size and redshift. This makes us suspicious that the potential correlation is caused by selection effects.

3.5. *Clusters with Wide-Angle–tailed Radio Galaxies*

Wide-angle–tailed radio galaxies (WATs) are an interesting, complex example of radio emission found in clusters (see, e.g., O'Donoghue, Owen, & Eilek 1990). These sources are interme-

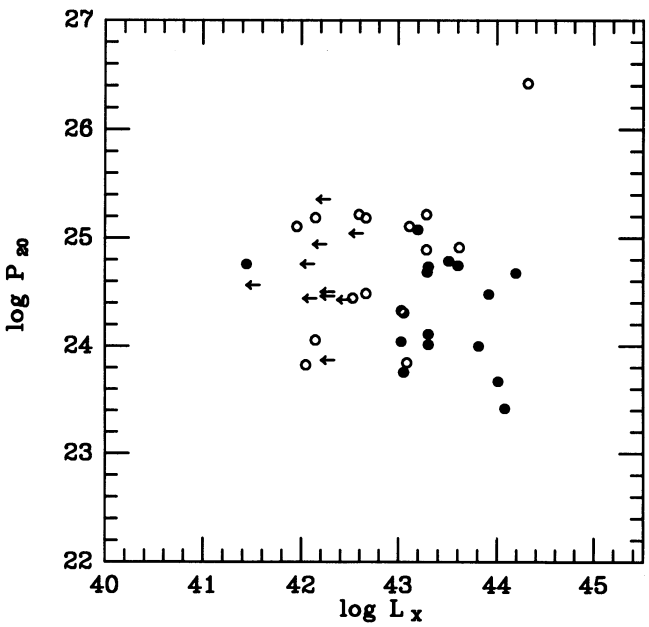

FIG. 3*a*

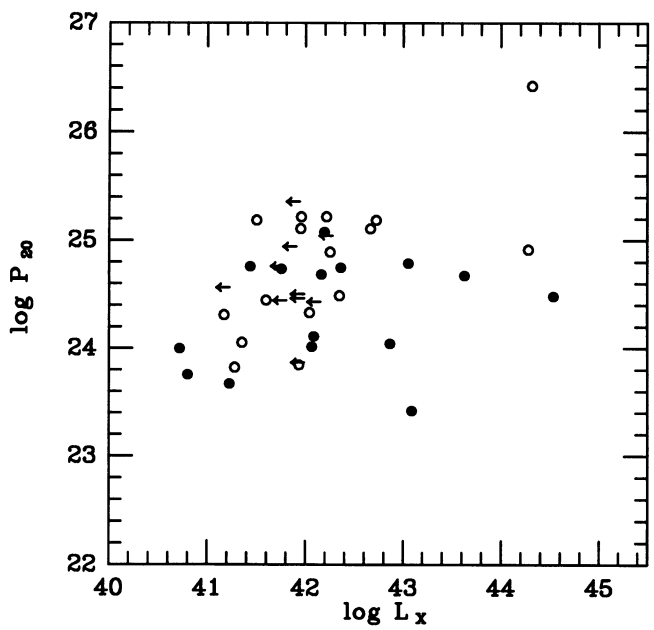

FIG. 3*b*

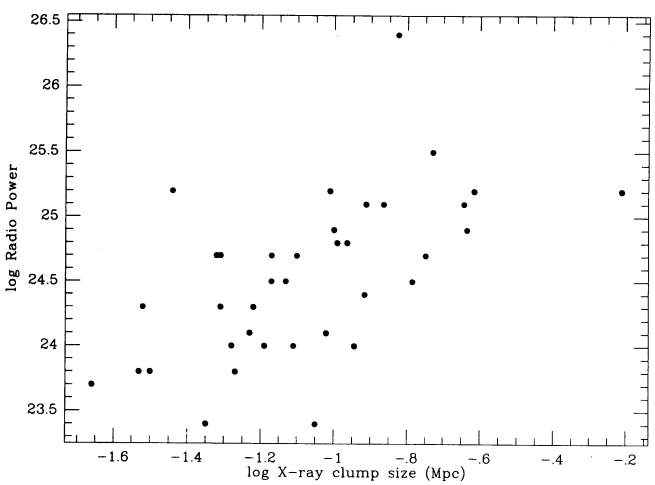

FIG. 3*c*

FIG. 3.—(*a*) Plot of the 20 cm radio power vs. cluster X-ray luminosity. The X-ray luminosity was measured down to an isophotal level of 3×10^{-3} counts s^{-1} arcmin^{-2}. The open circles are narrow-angle–tailed radio sources, and the filled circles are wide-angle–tailed radio galaxies and twin jet sources. (*b*) Same as (*a*), except the X-ray luminosity has been measured for the nearest X-ray subclump. (*c*) Plot of 20 cm radio power vs. X-ray clump size.

diate in radio power between Fanaroff & Riley (1974) classes I and II. They are associated with dominant central cluster galaxies (often D or cD). The radio structure consists of twin jets emerging from the radio galaxy which are straight and well collimated; the jets dramatically disrupt, often bend, and turn into diffuse, edge-darkened tails. For the O'Donoghue et al. (1990) sample, the median jet length is 36 kpc and the median total source diameter is 430 kpc. The origin of the jet disruption and bending is uncertain and has been the topic of much speculation (e.g., Eilek et al. 1984; Norman, Burns, & Sulkanen 1988). Unlike 70%–90% of optically similar clusters, WAT clusters (which are part of the Edge, Stewart, & Fabian 1992 sample, or which have been separately investigated, e.g., Burns et al. 1993) appear to have little evidence for X-ray cooling inflows (i.e., central cooling time is longer than a Hubble time).

We have seven to nine examples of WATs in the sample in Table 1. In nearly all these cases, the radio galaxies either appear offset from the local X-ray peak (by more than 30″, which is more than the typical error in the X-ray positions), as in A98, A400, A1569, A2220, and A2306, or have significant extensions or substructure near the radio galaxies, as in A690 and A2634. In two of these cases which have been studied most closely to date (A400, Owen, Eilek, & Burns 1994a; A2634, Burns et al. 1993), there are extensions of X-ray emission between the radio tails which lie well beyond the optical light distribution. These central X-ray structures in WAT clusters are unusual, since other optically similar clusters without WATs (e.g., A85 in Jones et al. 1979) typically have smooth centrally peaked X-ray emission at arcminute resolution.

We believe that this X-ray substructure is a signature of a relatively recent merger of a cluster with a group or subcluster. Very similar central substructure is seen in numerical simulations of cluster mergers which model both the gas and the dark matter (e.g., Evrard 1990; Roettiger, Burns, & Loken 1993). Some of the central substructure arises from shocks created during the mergers.

This merger model for WAT clusters has several attractive features. (1) It explains the unusual central X-ray substructure, which also does not appear to follow the optical light. (2) Cluster/subcluster mergers heat and expand the cluster core and, therefore, may destroy any cooling inflows in WAT clusters (Roettiger et al. 1993). (3) Large, residual gas motions ($\approx$800 km s^{-1}) persist in the cluster for 5 Gyr following a merger event; such large-scale motions may have enough ram pressure to bend the WAT jets/tails to their observed curvature. This is important, since the observed peculiar velocities of WATs alone (e.g., Pinkney et al. 1993) are insufficient to bend the jets/tails (Eilek et al. 1984). (4) The merging event itself may cause tidally stripped gas to accrete onto the core of the radio galaxy, thus triggering an AGN and the creation of a WAT. The nominal synchrotron lifetime of WATs (10^7–10^8 yr) is much less than the timescale for effects of the merger to dissipate (5×10^9 yr; Roettiger et al. 1993).

We are currently pursuing higher resolution *ROSAT* observations of these WAT clusters in an effort to confirm and extend the above observed trends and their interpretation.

3.6. *Orientations of Narrow-Angle–tailed Sources*

Narrow-angle–tailed radio galaxies (NATs) are radio sources with emission that trails off to one side of the optical galaxy (see, e.g., NATs in A1656 and A1589 in Fig. 1, and also O'Dea & Owen 1985). It is generally assumed that this head-tail radio morphology is produced by transonic motion of the radio galaxy through the ICM in which the resulting ram pressure sweeps radio plasma into the galaxy trail (or wake). However, this picture could be altered by interactions of radio jets with gas density enhancements around the radio galaxy. One way of investigating this is to examine the orientation of the radio tails, since they are most strongly influenced by local pressure gradients. O'Dea, Sarazin, & Owen (1987) previously studied the distribution of tail orientations with respect to the cluster centers for 70 NATs in an effort to investigate galaxy orbits in clusters. No strong conclusions were drawn from these data, although there is weak evidence for radial orbits of NATs closest to the cluster centers. Once again, might these statistics be influenced by local effects near the NATs?

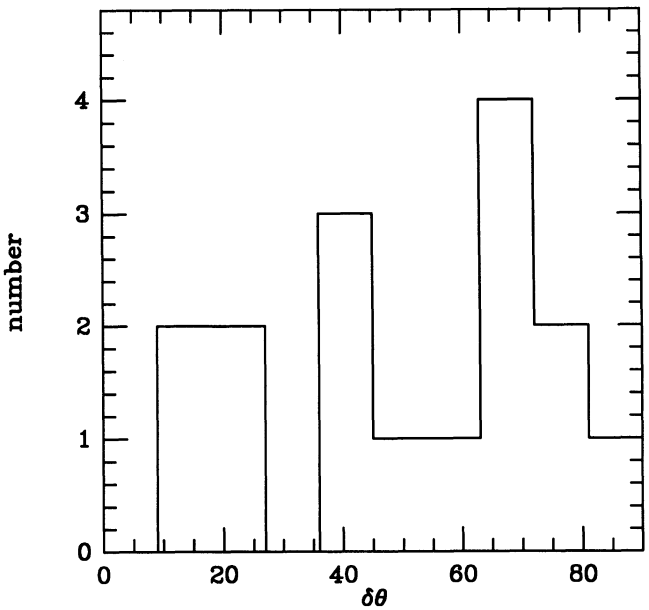

FIG. 4.—Distribution of angle differences ($\delta\theta$) for NATs; $\delta\theta$ is the difference between the position angle of the radio tail and the position angle of the line drawn between the radio galaxy and the nearest X-ray peak.

In Figure 4 we plot the distribution of tail angles measured relative to the line between the radio galaxy and the nearest X-ray subclump. A Kolmogorov-Smirnov test suggests that this histogram is consistent with a random distribution at the 60% confidence level. No strong alignment between the galaxy/clump and radio tail orientations is seen. Any effect would be difficult to see, however, because of projection effects, the small-number statistics, and the possible presence of AGN emission.

4. SUMMARY AND CONCLUSIONS

We have found a very strong correlation between the positions of radio galaxies and peaks or subclumps of X-ray emission within rich clusters of galaxies. Although radio galaxies are more strongly correlated with the centers of clusters than the general cluster galaxy distribution, the X-ray/radio coincidences are much stronger, and this distribution is not consistent with a King model. We considered three possible origins for the X-ray emission: free-free radiation from clumped hot gas within the cluster ICM, inverse Compton scattering of cosmic microwave photons by the relativistic electrons in the radio plasma, and nonthermal X-ray emission from AGNs. Although there is good evidence for an AGN component of

X-ray emission for some compact, high surface brightness regions where the X-ray peaks coincide with the radio galaxies, we believe that most of the X-ray emission around radio galaxies comes from hot gas in overdense subclumps surrounding the radio sources.

We also explored the relationship between the X-ray and radio luminosities. There does not appear to be any correlation between the radio power and the total cluster X-ray luminosity measured down to a constant isophotal level. This is consistent with previous results (e.g., Zhao et al. 1989). There are apparent correlations between the radio power and the X-ray luminosity of the local X-ray subclump, and between the radio power and the X-ray clump radius. However, we strongly suspect that these correlations may be artifacts of observational selection effects which also yield strong correlations of X-ray clump luminosity and clump size with redshift.

There are some interesting trends of radio morphology with X-ray emission. For example, we find that in clusters with wide-angle–tailed radio sources associated with optically dominant central galaxies, there is substantial X-ray substructure at the cluster core. This is unusual for clusters with dominant central galaxies where the X-ray emission is usually centrally peaked and smooth at arcminute resolution. However, we did not find any strong alignment between the radio tails for NATs and WATs and the position angle of the nearest X-ray subclump relative to the radio galaxy.

Do the above results help us to answer any of the questions about the nature of cluster radio galaxy emission posed in § 1? We believe so. In particular, it appears that the local gaseous environment in the immediate vicinity of radio galaxies is most important in influencing the observed radio properties rather than the global cluster environment. The X-ray subclumps probably act to shape and confine the radio plasma. So, if the local gaseous environment is the dominant influence and this local environment around radio galaxies is similar for both rich and poor clusters, this could explain the strong similarities in luminosity functions and in radio morphologies for radio galaxies in and out of Abell clusters. *Einstein* images (Price et al. 1991) and preliminary *ROSAT* images (Burns et al. 1993) of poor groups with extended radio sources do show strong evidence of clumped X-ray emission around radio galaxies similar to that seen in Figure 1 for Abell clusters.

Finally, what is the origin of the X-ray subclumps? Mergers between clusters would seem to be a good explanation. *N*-body simulations using a cold dark matter spectrum show that clusters grow hierarchically through the merger of groups and protoclusters (e.g., Evrard, Summers, & Davis 1992). The increasing frequency of subclustering seen on optical images (e.g., Fitchett & Webster 1987; Rhee, van Haarlem, & Katgert 1991b; Beers et al. 1991) and X-ray images (Forman & Jones 1990; Briel et al. 1991; Briel, Henry, & Böhringer 1992; Davis & Mushotzky 1993; White, Briel, & Henry 1993) would seem to support the idea that such mergers are taking place even today. The X-ray properties of clusters with merging subcomponents agree well with recent numerical *N*-body + hydrodynamics simulations of merging clusters (Evrard 1990; Roettiger et al. 1993). Also, the apparent evolution of the X-ray luminosity function (Edge et al. 1990) and the numbers of X-ray cooling flow clusters (Donahue, Stocke, & Gioia 1992) with z have been interpreted in terms of this merging scenario. From the data presented in this paper, it further appears that radio galaxies are excellent markers of clusters or regions within clusters where subclustering and merging have occurred. The production and evolution of the extended radio plasma may very well be stimulated by the merging process. Therefore, radio galaxies in clusters should be viewed with renewed interest as important tools in probing the evolution of structure within clusters.

This work was supported by NSF grant AST-9012353 and a NASA Long Term Space Astrophysics grant NAGW-3152. We thank the CfA for providing the X-ray images on CD ROM, and Eric Feigelson and his colleagues for their ASURV statistical package. We also thank Chris Loken, Kurt Roettiger, Anatoly Klypin, John Stocke, and the referee, Chris O'Dea, for useful conversations and constructive comments on the text.

APPENDIX

COMMENTS ON INDIVIDUAL CLUSTERS

Abell 74.—A74 has several radio sources in the direction of this cluster. The westernmost and easternmost radio sources are not identified with cluster galaxies. Only the central NAT radio source, which also coincides with the X-ray peak, is associated with a cluster galaxy ($m = 14.5$ mag, estimated from the Palomar Sky Survey (POSS) E prints as in Papers I–III). The Abell center is displaced about 3.'5 from the X-ray peak.

Abell 75.—The radio source in A75 is classified as a somewhat unusual diffuse double with relatively weak lobes and lobe hot spots. The optical identification is a 15.1 mag galaxy located between the radio lobes and is 0.07 Abell cluster radii from the Abell center. The X-ray image reveals statistically significant substructure (both the southeastern and western X-ray clumps meet our criteria for a "real" clump), although the X-ray subclumps are not closely aligned with the radio morphology. There are several bright galaxies that lie near the eastern X-ray peak ($\alpha = 00^h37^m08^s$, $\delta = 20°56'$) as seen on the Palomar Sky Survey (POSS) E print.

Abell 98.—A98 has a bimodal distribution of X-ray emission (Forman et al. 1981; Henry et al. 1981) and optical galaxies (Beers & Tonry 1986; Zabludoff, Huchra, & Geller 1990). The X-ray and radio emissions shown in Figure 1 are centered on the southernmost subcluster of galaxies (the northern subcluster is off this image). The cross represents the Abell center of A98. This subcluster itself is further divided into two significant X-ray components where the radio galaxy is closest to the X-ray peak at $\alpha = 00^h43^m48^s$. The radio source is identified with a 14.7 mag ($M = -23.5$ mag) optically bright galaxy, and the radio morphology is classified as a WAT. There is a clumping of galaxies near the radio source and its associated X-ray component, but no obvious collection of galaxies associated with the X-ray peak at $\alpha = 00^h43^m57^s$ as seen on the POSS print.

Abell 114.—The twin jet radio source in Figure 1 appears to be associated with a possible X-ray clump which is formally significant at the 2 σ level. However, the strong spatial coincidence between the X-ray and the radio emission lends additional credibility to this association. The optical galaxy lies at a distance of 0.12 Abell cluster radii from the cluster center and has a magnitude of 14.5 ($M = -22.4$ mag). The X-ray clumps to the south (at $\alpha = 00^h51^m05^s$) and the southeast (at $\alpha = 00^h51^m20^s$) of the radio source are statistically significant.

Abell 133.—A133 contains a very interesting, steep-spectrum radio source (see also Slee & Reynolds 1984) classified by Burns (1990) as amorphous. The cD galaxy ($m = 13.0$ mag), which coincides with the X-ray peak, is centered on the compact radio extension $\approx 40''$ to the south of the main radio "lobe" ($\alpha = 01^h00^m15^s.4$, $\delta = -22°09'$). Arnaud (1989) reports a 134 $M_\odot$ yr^{-1} cooling flow in this cluster. There are also optical emission-line filaments visible in and around the cD (Hu, Cowie, & Wang 1985; Sarazin & Graney 1991).

Abell 160.—A160 contains a WAT (O'Donoghue et al. 1990) associated with an optically dominant, multiple-nucleus (Valentijn & Casertano 1988) galaxy ($m = 13.7$ mag). The X-ray peak closest to the radio galaxy is only significant on the 2.3 σ level. However, the more compact X-ray emission to the northeast of the radio galaxy is statistically significant.

Abell 194.—This cluster shows good evidence of multiple X-ray substructures (Beers & Tonry 1986). Both the high surface brightness peak near the TJ radio galaxy and the X-ray "extension" near the NAT are significantly above the surrounding background. The optical identification for the eastern radio source is NGC 547, a 12.0 mag galaxy. The western NAT is identified with NGC 541, a 13.0 mag galaxy (O'Dea & Owen 1985); this radio source may have been responsible for triggering star formation in the nearby "Minkowski's object" (Brodie, Bowyer, & McCarthy 1985; van Breugel et al. 1985).

Abell 400.—This unusual multitailed twin jet source, 3C 75, is identified with the dumbbell galaxy ($m = 14.0$ mag) at the optical center of A400. Owen et al. (1985) presented detailed VLA images of this radio source. The X-ray emission appears to be slightly elongated in a direction parallel to the radio tails (McMillan, Kowalski, & Ulmer 1989), similar to that seen in other WATs. Also, there is no evidence for a strong X-ray cooling flow in this cluster (Arnaud 1989). Beers et al. (1992) recently reported multiple galaxy velocity systems in this cluster, possibly centered around the radio nuclei.

Abell 401.—The cD galaxy at the optical/X-ray center of A401 is radio-quiet (Burns & Ulmer 1980). However, there are two NATs associated with elliptical galaxies outside the cluster core. The western NAT is identified with a 15.2 mag galaxy, and the identification for the eastern NAT has $m = 15.0$ mag. There is some suggestion of a ridge of X-ray emission near the eastern NAT, but it is not statistically significant. Arnaud (1989) and Edge et al. (1992) report a weak cooling flow within this cluster (15 $M_\odot$ yr^{-1}). White et al. (1991) note the presence of cold X-ray absorbing gas in the cluster center. Sarazin & Graney (1991) find an extended optical emission-line system associated with the cD.

Abell 407.—A structurally complex radio source coincides with the X-ray peak in A407. The optical identification is a bright dumbbell galaxy (Valentijn & Casertano 1988) with $m \approx 15.0$ mag. The optical halo of this galaxy contains at least eight possible nuclei (Schneider & Gunn 1982).

Abell 415.—This possible NAT ($m = 14.0$ mag) is about 4′, or 0.16 Abell radii, from the cluster center, and about 8′ south of the cD galaxy (Ball, Burns, & Loken 1993). There is a strong peak of X-ray emission less than 1′ away from the radio galaxy position. The cD in A415 is radio-quiet.

Abell 514.—There are three tailed radio sources in this cluster, each associated with moderate-brightness optical galaxies ($m \approx 14.5$ mag, $M \approx -22$ mag). Each tailed source is within $\approx 2'$ of a significant X-ray peak. Overall, there is an elongation of X-ray emission in Figure 1, and optical galaxies (Rhee & Katgert 1987) stretch between the southern and northern radio galaxies.

Abell 569.—The broad, twin jet radio source is identified with one of several bright galaxies (NGC 2329) in this nearby cluster ($m = 11.9$ mag, $M = -22.7$ mag). A569 may be part of a northern extension of the Perseus-Pisces supercluster (e.g., Batuski & Burns 1985; Chamaraux et al. 1990). The X-ray emission is relatively compact, high surface brightness, and centered on the radio galaxy.

Abell 629.—There are two tailed radio sources in this cluster. The northern NAT is identified with a 15.7 mag galaxy, and the southern tailed source is identified with a 16.5 mag galaxy in this relatively distant cluster. There is some suggestion of an extension of the X-ray emission in the direction of the southern radio source.

Abell 690.—A690 contains a dramatic example of a giant WAT (O'Donoghue et al. 1990) identified with a cD galaxy ($m = 13.9$ mag, $M = -23.8$ mag). The X-ray core has an elongation in a direction between the radio tails. We treat this central X-ray emission as a single component in Table 1. The cluster X-ray luminosity is unusually low for a cluster with a dominant galaxy and a wide-angle–tailed radio source.

Abell 780.—The central radio source in A780 is Hydra A (Taylor et al. 1990). The optical identification is very bright ($m = 13.2$ mag, -24.0 mag) and coincides with the X-ray peak. This cluster also has a very strong cooling flow (600 $M_\odot$ yr^{-1}) inferred from the high central X-ray surface brightness (David et al. 1990). Although the radio morphology of Hydra A resembles a WAT, its radio power is much larger than that typically found for WATs (see Table 1).

Abell 1234.—This distant cluster has a complex, probably tailed, radio source associated with a 15.8 mag galaxy. There is significant X-ray substructure within the cluster, including a 3 σ X-ray peak 1′ to the southwest of the radio galaxy position. The X-ray extension to the southeast of the radio galaxy is also clearly real, as is the compact, high surface brightness X-ray structure to the northwest.

Abell 1367.—A1367 is one component on the Coma-A1367 supercluster (Chincarini, Giovanelli, & Haynes 1983; Gregory, Tifft, & Moody 1988). Both the optical galaxies (e.g., Rhee et al. 1991a) and the X-ray emission (Bechtold et al. 1983) show an elongated structure running from the southeast to the northwest. A compact, high surface brightness X-ray peak is centered on the NAT ($m = 13.3$ mag), 3C 264 (Gavazzi & Jaffe 1986), at the southeast extremity of the cluster. There is also an interesting collection of weaker radio galaxies within an X-ray subclump at the northwest extremity.

Abell 1425.—A1425 is one of the few clusters in this sample that contains a classical double radio source. The source is identified

with a 16.5 mag, nondominant cluster galaxy. There is no detectable diffuse X-ray emission on the *Einstein* image for this relatively distant cluster.

Abell 1446.—This cluster contains another example of a WAT (O'Donoghue et al. 1990) identified with a 14.8 mag ($M = -23.4$ mag) giant elliptical which lies at the peak of the cluster X-ray emission.

Abell 1569.—The X-ray emission for A1569 is clearly bimodal in Figure 1. An examination of the POSS print also shows that there are two clumps of galaxies which coincide with the X-ray concentrations. The southern X-ray clump is the home of a WAT ($m = 14.3$ mag); the WAT appears to lie along an X-ray ridge between two more compact, significant X-ray components. The northern X-ray clump contains a twin jet source which is identified with an even more optically luminous galaxy ($m = 13.7$ mag).

Abell 1589.—The NAT is associated with a relatively bright (14.0 mag) galaxy to the southwest of the cluster center. There is an extension of X-ray emission in the direction of the NAT. In Table 1 we summed the X-ray emission within a circle that includes the two westernmost X-ray peaks nearest the radio galaxies; this "extension" is significant on the 2.8 σ level. There is also a clumping of galaxies along this X-ray extension on the POSS print.

Abell 1656 (Coma).—There are two radio sources shown on the image of Coma in Figure 1. The smaller, northern radio source (which is less than 2′ in diameter and does not meet the condition for inclusion in Table 1) is associated with one of the two D galaxies ($m = 11.9$ mag) that lies within the core of the cluster, and coincides with a statistically significant X-ray peak. The NAT (O'Dea & Owen 1985; Feretti et al. 1990) is identified with a less bright, but still prominent, elliptical galaxy ($m = 13.6$ mag, $M = -21.5$ mag). The optical galaxy, which lies at the "head" of the NAT, also closely coincides with a compact X-ray component that is significant on the 3.4 σ level. There is no evidence for a cooling flow in A1656, but there is significant X-ray substructure (Briel et al. 1992; White et al. 1993).

Abell 1736.—The radio sources in Figure 1 appear to be associated with two clusters. The main cluster to the north contains two tailed radio sources: a faint NAT at $\alpha = 13^h24^m$, $\delta = -26°.7$, identified with a 15.2 mag galaxy, and a bright NAT closer to the cluster center at $\alpha = 13^h24^m$, $\delta = -26°.8$, identified with a 13.6 mag E galaxy. The NATs have redshifts of 0.0483 and 0.0436, respectively. The tailed radio sources in the southwest corner of the image (13^h23^m, $-27°.1$), associated with a clump of X-ray emission, appear to be identified with a foreground cluster at $z \approx 0.035$.

Abell 1775.—A1775 contains two separate radio galaxies, one compact and one extended, as discussed in O'Dea & Owen (1985) and in Paper III. These radio galaxies may be nuclei of a bright ($m \approx 13.3$ mag) dumbbell galaxy. This cluster does not appear to have an X-ray cooling inflow (Arnaud 1989).

Abell 1836.—There is a weak (2.8 σ) X-ray detection of the AGN associated with the radio galaxy and possibly extended X-ray emission as well. The edge-brightened radio double in A1836 is identified with a 12.8 mag ($M = -23.2$ mag) galaxy which lies at the optical center of this Abell cluster. The X-ray luminosity of this cluster is low (3×10^{41} ergs s^{-1}).

Abell 1890.—The twin jet or WAT radio source in A1890 is associated with a giant E or cD galaxy ($m = 16.0$ mag) which lies near the X-ray centroid. Individual X-ray peaks other than the X-ray centroid are not statistically significant; however, there is a clear elongation oriented between the radio tails. There is no evidence of a cooling flow in A1890 (Arnaud 1989).

Abell 1939.—A1939 contains two twin jet radio sources identified with 15.5 mag (14^h35^m, $+24°.9$) and 15.2 mag (14^h35^m, $+25°.0$) galaxies. No significant cluster X-ray emission was detected by *Einstein.*

Abell 2022.—This cluster contains an excellent example of a U-shaped NAT (15^h02^m, $+28°.7$). The optical galaxy ($m = 14.7$ mag) has a redshift of 0.0452, which is significantly less than the mean cluster redshift (0.0575), suggesting a velocity difference of 3700 km s^{-1}. There is a significant, resolved clump of X-ray emission to the south of the radio source (at 15^h02^m, $+28°.8$), although there is also an interesting but very weak (and not statistically significant) X-ray peak very close to the radio galaxy ($m = 14.4$ mag) in Figure 1.

Abell 2147.—A2147 is part of the Hercules supercluster (e.g., Batuski & Burns 1985). There is a very unusual diffuse radio source which lies to the southeast of the cluster center in Figure 1. The optical identification for this radio source remains unclear, since there is no compact radio component with which to associate a single galaxy. Our new result in Figure 1 is that there is a quite significant ridge of X-ray emission which extends toward and surrounds this diffuse radio source.

Abell 2162.—A2162 is also in the Hercules supercluster complex. However, there is little or no X-ray emission detected by *Einstein* in Figure 1 for this cluster. There is a 2.5 σ X-ray peak near the southernmost radio galaxy ($m = 12.7$ mag, $M = -22.9$ mag). This is another example of a double-lobe radio source associated with a low X-ray luminosity cluster.

Abell 2220.—The relationship between the X-ray and radio emission in this cluster was previously discussed by Burns & Balonek (1982). The radio source is a WAT associated with a bright (6.0 mag) galaxy in the cluster. There is significant X-ray subclumping near the radio galaxy.

Abell 2256.—*ROSAT* observations of A2256 were reported by Briel et al. (1991). They find excellent evidence for significant subclustering which has been interpreted as the infall of a smaller, cooler cluster into a larger, hotted cluster. There is an interesting alignment of radio sources near the purported bow shock of the smaller cluster (Henry & Briel 1991). A2256 does not have a cooling inflow.

Abell 2306.—This distant cluster ($z = 0.257$) contains a WAT associated with the dominant cluster galaxy (15.5 mag) which lies very near the western X-ray peak. The X-ray luminosity is moderate (4×10^{43} ergs s^{-1}). The secondary X-ray clump to the east of the radio galaxy is statistically significant and is not associated with an obvious collection of cluster galaxies on the POSS.

Abell 2634.—A2634 contains the prototype WAT 3C 465 (NGC 7720) (Leahy 1984), identified with a cD galaxy ($m = 12.2$ mag) which lies at the X-ray centroid. Eilek et al. (1984) previously compared the X-ray and radio emission for this cluster. They found an elongated, asymmetric X-ray extension between the radio tails which was recently confirmed by *ROSAT* (Burns et al. 1993). Our sample in Figure 1 suggests that such X-ray extensions are common for WAT clusters. There is also no evidence for a cooling flow in this cluster. Pinkney et al. (1993) recently reported that the cD in A2634 has a peculiar velocity of ≈ 200 km s^{-2} with respect to the cluster centroid. A second, twin jet radio galaxy (23^h37^m, $+26°.8$; NGC 7728, $m = 13.0$ mag), which lies at 0.39 Abell cluster radii from the cluster center (not shown in Fig. 1), also has an X-ray peak nearby.

REFERENCES

Abell, G. O. 1958, ApJS, 3, 211
Abell, G. O., Corwin, H. G., & Olowin, R. P. 1989, ApJS, 70, 1
Arnaud, K. A. 1989, private communication
Ball, R., Burns, J. O., & Loken, C. 1993, AJ, 105, 53
Batuski, D. J., & Burns, J. O. 1985, AJ, 90, 1413
Bechtold, J., Forman, W., Giacconi, R., Jones, C., Schwarz, J., Tucker, W., & van Speybroeck, L. 1983, ApJ, 265, 26
Beers, T. C., Forman, W., Huchra, J. P., Jones, C., & Gebhardt, K. 1991, AJ, 102, 1581
Beers, T. C., Gebhardt, K., Huchra, J. P., Forman, W., Jones, C., & Bothun, G. D. 1992, ApJ, 400, 410
Beers, T. C., & Tonry, J. L. 1986, ApJ, 300, 557
Binney, J., & Tremaine, S. 1987, Galactic Dynamics (Princeton: Princeton Univ. Press)
Birkinshaw, M., & Worrall, D. M. 1993, ApJ, 412, 568
Briel, U., et al. 1991, A&A, 246, L10
Briel, U. G., Henry, J. P., & Böhringer, H. 1992, A&A, 259, L31
Brodie, J. P., Bowyer, S., & McCarthy, P. 1985, ApJ, 293, L59
Brown, D. L., & Burns, J. O. 1991, AJ, 102, 1917
Burns, J. O. 1990, AJ, 99, 14
Burns, J. O., & Balonek, T. J. 1982, ApJ, 263, 546
Burns, J. O., Gregory, S. A., & Holman, G. D. 1981, ApJ, 250, 450
Burns, J. O., Hanisch, R. J., White, R. A., Nelson, E. R., Morrisette, K. A., & Moody, J. W. 1987, AJ, 94, 587
Burns, J. O., Rhee, G., Roettiger, K., & Owen, F. N. 1993, in ASP Conf. Ser. 51, Observational Cosmology, ed. G. Chincarini, A. Iovino, T. Maccacaro, & D. Maccagni (San Francisco: ASP), 407
Burns, J. O., & Ulmer, M. P. 1980, AJ, 85, 773
Chamaraux, P., Cayatte, V., Balowski, C., & Fontanelli, P. 1990, A&A, 229, 340
Chincarini, G. L., Giovanelli, R., & Haynes, M. P. 1983, A&A, 121, 5
Crawford, C. S., & Fabian, A. C. 1993, MNRAS, 260, L15
Daly, R. A. 1992, ApJ, 399, 426
David, L. P., Arnaud, K. A., Forman, W., & Jones, C. 1990, ApJ, 356, 32
Davis, D. S., & Mushotzky, R. F. 1993, AJ, 105, 409
Donahue, M., Stocke, J. T., & Gioia, I. M. 1992, ApJ, 385, 49
Edge, A. C., Stewart, G. C., & Fabian, A. C. 1992, MNRAS, 258, 177
Edge, A. C., Stewart, G. C., Fabian, A. C., & Arnaud, K. A. 1990, MNRAS, 245, 559
Eilek, J. A., Burns, J. O., O'Dea, C. P., & Owen, F. N. 1984, ApJ, 278, 37
Evrard, A. E. 1990, ApJ, 363, 349
Evrard, A. E., Summers, F. J., & Davis, M. 1992, preprint
Fabbiano, G. 1989, ARA&A, 27, 87
Fabbiano, F., Miller, L., Trinchieri, G., Longair, M., & Elvis, M. 1984, ApJ, 277, 115
Fabian, A. C., Nulsen, P. E. J., & Canizares, C. R. 1991, Astron. Astrophys. Rev., 2, 191
Fanaroff, B. L., & Riley, J. M. 1974, MNRAS, 167, 31P
Fanti, C., et al. 1983a, A&AS, 51, 179
———. 1983b, A&AS, 52, 411
Fanti, R. 1984, in Clusters and Groups of Galaxies, ed. F. Mardirossian, G. Giuricin, & M. Mezzetti (Boston: Reidel), 185
Feigelson, E., & Berg, C. 1983, ApJ, 269, 400
Feigelson, E. D., & Nelson, P. I. 1985, ApJ, 293, 192
Feretti, L., Dallacasa, D., Giovannini, G., & Venturi, T. 1990, A&A, 232, 337
Fichett, M., & Webster, R. 1987, ApJ, 317, 653
Forman, W., Bechtold, J., Blair, W., Giacconi, R., van Speybroeck, L., & Jones, C. 1981, ApJ, 243, L133
Forman, W., & Jones, C. 1982, ARA&A, 20, 547
———. 1990, in STScI Symp. 4, Clusters of Galaxies, ed. W. R. Oegerle, M. J. Fitchett, & L. Danly (Cambridge: Cambridge Univ. Press), 287
Gavazzi, G., & Jaffe, W. 1986, ApJ, 310, 53
Gregory, S. A., Tifft, W. G., & Moody, J. W. 1988, AJ, 95, 662
Harris, D. E., et al. 1990, The *Einstein Observatory* Catalog of IPC X-Ray Sources (Washington, DC: SAO)
Henry, J. P., & Briel, U. G. 1991, A&A, 246, L14
Henry, J. P., Henriksen, M. J., Charles, P. A., & Thorstensen, J. R. 1981, ApJ, 243, L137
Hu, E. M., Cowie, L. L., & Wang, Z.-H. 1985, ApJS, 59, 447
Isobe, T., & Feigelson, E. D. 1990, BAAS, 22, 917
Jedrzejewski, R. 1987, MNRAS, 226, 747
Jones, C., Mandel, E., Schwarz, J., Forman, W., Murray, S. S., & Harnden, F. R. 1979, ApJ, 234, L21
Jones, T., & Owen, F. N. 1979, ApJ, 234, 818
Leahy, P. 1984, MNRAS, 208, 323
Mauche, C. W., & Gorenstein, P. 1986, ApJ, 302, 371
McMillan, S. L. W., Kowalski, M. P., & Ulmer, M. P. 1989, ApJS, 70, 723
Mohr, J. J., Fabricant, D. G., & Geller, M. J. 1993, preprint
Morganti, R., Fanti, R., Gioia, I. M., Harris, D. E., Parma, P., & de Ruiter, H. 1988, A&A, 189, 11
Norman, M. L., Burns, J. O., & Sulkanen, M. 1988, Nature, 335, 146
O'Dea, C. P. 1985, ApJ, 295, 80
O'Dea, C. P., & Owen, F. N. 1985, AJ, 90, 954
O'Dea, C. P., Sarazin, C. L., & Owen, F. N. 1987, ApJ, 316, 113
O'Donoghue, A. A., Owen, F. N., & Eilek, J. A. 1990, ApJS, 72, 75
Owen, F. N., Eilek, J. A., & Burns, J. O. 1994a, in preparation
Owen, F. N., Ledlow, M., & Keel, W. 1994b, in preparation
Owen, F. N., O'Dea, C. P., Inoue, M., & Eilek, J. 1985, ApJ, 294, L85
Owen, F. N., White, R. A., & Burns, J. O. 1992, ApJS, 80, 501 (Paper II)
Owen, F. N., White, R. A., & Ge, J.-O. 1993, ApJS, 87, 135 (Paper III)
Owen, F. N., White, R. A., Hilldup, K. C., & Hanisch, R. J. 1982, AJ, 87, 1063
Owen, F. N., White, R. A., & Thronson, H. 1988, AJ, 95, 1
Pacholczyk, A. G. 1970, Radio Astrophysics (San Francisco: Freeman)
Pinkney, J., Rhee, G., Burns, J., Hill, J., Oegerle, W., Batuski, D., & Hintzen, P. 1993, ApJ, 416, 36
Price, R., Burns, J. O., Duric, N., & Newberry, M. V. 1991, AJ, 102, 14
Raymond, J. C., & Smith, B. W. 1977, ApJS, 35, 419
Rhee, G., Burns, J. O., & Kowalski, M. 1994, in preparation
Rhee, G., & Katgert, P. 1987, A&A, 183, 217
Rhee, G., van Haarlem, M. P., & Katgert, P. 1991a, A&AS, 91, 513
———. 1991b, A&A, 246, 301
Roettiger, K., Burns, J. O., & Loken, C. 1993, ApJ, 407, L53
Sarazin, C. L. 1986, Rev. Mod. Phys., 58, 1
Sarazin, C. L., & Graney, C. M. 1991, ApJ, 375, 532
Schneider, D. P., & Gunn, J. 1982, ApJ, 263, 14
Slee, O. B., & Reynolds, J. E. 1984, Proc. Astron. Soc. Australia, 5, 516
Stark, A. A., Gammie, C. F., Wilson, R. W., Bally, J., Linke, R. A., Heiles, C., & Hurwitz, M. 1992, ApJS, 79, 77
Stocke, J., & Burns, J. O. 1987, 319, 671
Struble, M. F., & Rood, H. J. 1991, ApJS, 77, 363
Tananbaum, H., et al. 1979, ApJ, 234, L9
Taylor, G. B., Perley, R. A., Inoue, M., Kato, T., Tabara, H., & Aizu, K. 1990, ApJ, 360, 41
Tucker, W. H. 1975, Radiation Processes in Astrophysics (Cambridge: MIT)
Valentijn, E. A., & Caserano, S. 1988, A&A, 206, 27
van Breugel, W., Filippenko, A. V., Heckman, T., & Miley, G. 1985, ApJ, 293, 83
White, D. A., Fabian, A. C., Johnstone, R. M., Mushotzky, R. F., & Arnaud, K. A. 1991, MNRAS, 252, 72
White, S. D. M., Briel, U. G., & Henry, J. P. 1993, MNRAS, 261, L8
Zabludoff, A. I., Huchra, J. P., & Geller, M. J. 1990, ApJS, 74, 1
Zhao, J.-H., Burns, J. O., & Owen, F. N. 1989, AJ, 98, 64 (Paper I)